MAGMA IN EARTH'S LOWER MANTLE: FIRST PRINCIPLE MOLECULAR DYNAMICS SIMULATIONS OF SILICATE LIQUIDS

by

Ni Sun

A dissertation submitted in partial fulfillment
of the requirements for the degree of
Doctor of Philosophy
(Geology)
in The University of Michigan
2008

Doctoral Committee:

Professor Lars P. Stixrude, Co-chair
Professor Rebecca A. Lange, Co-chair
Professor Lynn M. Walter
Professor Youxue Zhang
Assistant Professor Anton van der Ven

To Xiqiao and Our Families

ACKNOWLEDGEMENTS

First, I would like to thank my Ph.D. advisor, Lars Stixrude, for his years of mentoring and supervision. He attracted me to the field of computational mineral physics with his scientific enthusiasm, critical thinking, and hard working, which have influenced me all along with my education at the University of Michigan. He not only deeply understands physics and geology, but also could express and explain complex matters in an easily understandable way.

I would also like to thank other committee members: Becky Lange, Youxue Zhang, Lynn Walter, and Anton van der Ven. I am very grateful to Becky not only for her being one of the co-chairs of my committee but also for her valuable advice and continued interest in my research. Thanks Youxue for his detailed discussions and patient answers to my questions. Thanks Lynn for her continued support and helpful comments. Also thanks Anton, my cognate committee member, to provide helpful insights and fresh perspectives on geological problems.

I am very grateful to my colleagues, Professor Bijaya Karki from Louisiana State University, Nico de Koker, Stephen Stackhouse, and Mainak Mookherjee, for their help and contributions to some projects of my research.

I want to thank professors in geophysics, Carolina Lithgow-Bertelloni, Larry Ruff, Jeroen Ritsema, and Peter van Keken, for their comments and discussions in the

broad geological topics in Friday geophysics meeting. Also thanks to geophysics students and post-docs, past or present, Katie Davis, Wendy Panero, Wenbo Xu, Yang Zhang, Xin Wan, Xin Wang, Hans Hiser, Yong Keun Hwang, John Naliboff, and J.P. Brandenburg. Thanks for their support and friendship and making the Friday geophysics meetings more and more interesting and informative.

And many other past or present graduate students and post-docs, Qiong Liu, Yuhui Ai, Jing Zhou, Yang Chen, Wenjun Yong, Maodu Yan, Hejiu Hui, Huaiwei Ni, Tie Sun, and Yuehan Lu, are appreciated for their friendship and encouragement. They are always there – attending my practice talks, giving suggestions and ideas of improvement whenever I need them. I also want to thank all the people in the department of Geological Sciences who provide great environment that gave me unforgettable memory here. In particular, the weekly Friday afternoon talks, which invite outstanding geologists from all over the world and attract full attendance of the whole department, have so effectively broaden scope of my knowledge and deepen understanding of varies aspects of geology.

Also thanks my best friends in Ann Arbor, Yunyan Tao, Zhibin Yang, and Xiaotong Zhang, who gave me emotional support and always with me whether I am happy or sad. Thanks my cousins, Dan and Jing, who are also living in Ann Arbor. They are always in front of me when I met difficulties.

My deepest and warmest gratitude go to my husband, Xiqiao, and our families. Thanks Xiqiao for his ten years of encouragement, support, and love all the way from Beijing to Ann Arbor. His complete confidence in me had kept me going through the hardest times. And he can make great meals! My parents, my sister, Ying, and my brother

in law, Zhong, have been critically important for me to finish my Ph.D. study. Thanks for their unconditional love. Also, many thanks to my parents in law for their continued care and support.

TABLE OF CONTENTS

LIST OF FIGURES

Figure

LIST OF TABLES

Table

ABSTRACT

MAGMA IN EARTH'S LOWER MANTLE: FIRST PRINCIPLE MOLECULAR DYNAMICS SIMULATIONS OF SILICATE LIQUIDS

by

Ni Sun

Co-Chairs: Professor Lars P. Stixrude and Professor Rebecca A. Lange

$CaMgSi_2O_6$ and $CaSiO_3$ liquids have been investigated over the entire mantle pressure regime using first principles molecular dynamics simulations with density functional theory in the local density approximation and the ultra-soft plane-wave pseudopotential method. The equilibrated liquid structure is much more densely packed at high pressure. The average Si-O coordination number increases nearly linearly from 4 to 6 with compression. The results are well fitted by Mie-Grüneisen equation of state, $P(V,T) = P_C(V,T_0) + P_{TH}(V,T)$, with a Grüneisen parameter that linearly increases and heat capacity that linearly decreases with compression. The total and self diffusion coefficients of diopside liquid exhibit an unusual pressure dependence, first decreasing with increasing pressure, than increasing, and finally decreasing again at the highest pressures. This pattern is explained by the pressure-induced decrease in the number of excess non-bridging oxygens at low pressure, and the increase in the number of 5-fold coordinated silicons at higher pressures. Mg has a slightly higher self-diffusion coefficient than Ca, both of which are slightly more diffusive than O and Si. The average activation energy over the temperature range 3000-6000 K is lower than that found

experimentally at lower temperatures, consistent with non-Arrhenian behavior. We combine our results with previous results on $MgSiO_3$ composition to determine the volume of mixing on the $MgSiO_3$-$CaSiO_3$ join. The volume of mixing is zero within uncertainty.

CHAPTER I

INTRODUCTION

The Earth's crust, including continental and oceanic regions, is the product of partial melting. Indeed, silicate liquids are primary agents of terrestrial chemical differentiation. The processes of magma generation and transport responsible for the formation of the crust occur primarily in the shallow mantle and lithosphere at depths less than 200 km (6 GPa). In this regime, melting occurs primarily by decompression, or the addition of volatiles.

There is increasing evidence that melt may exist in Earth at depths much greater than the present day shallow magma genetic zone. The mechanism by which deep melt is generated may be fundamentally different. For example, melt is now thought to exist at the core-mantle boundary (136 GPa, 2890 km depth), where it may be stabilized by the thermal boundary layer at the base of the mantle, and the resulting high temperature, which may exceed the adiabat by more than 1,000 K (Williams and Garnero, 1996). Other lines of evidence for deep melt, include xenoliths that have originated at depths of 300 km or more (Haggerty and Sautter, 1990), and ancient magma genesis, including komatiites (Herzberg, 1995; Miller et al., 1991). Giant-impact models of lunar formation (Benz et al., 1986; Canup and Asphaug, 2001), suggest that the Earth was completely

molten in its earliest stages, and that crystallization from this initially molten state may have profoundly influenced the subsequent structure, dynamics, and evolution of Earth's mantle and core.

In order to understand the origin and significance of deep melt in the present day Earth, and the greater role of melts in the ancient, presumably hotter Earth, it is crucial to obtain accurate constraints on thermodynamic and dynamic parameters at high pressure and high temperature. Despite their importance in geological processes, very little is known of silicate melts at pressures beyond that of the present-day magma genetic regime (few GPa).

Here, silicate liquids are investigated across the entire mantle pressure-temperature regime by first principles molecular dynamics (FPMD) simulations, which have been successfully used to study silicate liquids (de Koker et al., 2008; Stixrude and Karki, 2005) and which allow us to predict physical properties of silicate liquids at high pressure and temperature. In this thesis, I will especially focus on diopside ($CaMgSi_2O_6$) liquid and wollastonite ($CaSiO_3$) liquid. These, together with $MgSiO_3$, account for 80 % of the bulk silicate Earth. Diopside is a major component of basalt and has been widely studied, including by shock wave experiments up to 40 GPa. These compositions allow us to investigate the thermodynamics of mixing of silicate liquids at high pressure, about which very little is known, on a simple homovalent join: $MgSiO_3$-$CaSiO_3$ at high pressure.

The goals of this thesis are to provide state-of-the-art theoretical predictions of the properties of silicate liquids that must form a basis for any discussion of their role in geological processes, including the structure, equation of state, and transport properties

over the whole mantle regime. I will also compare with existing experimental data in order to test the fundamental theories upon which my calculations are based, and to point the way towards future experiments at higher pressure.

Previous experimental studies provide well characterized physical and thermodynamic properties of diopside liquid at ambient pressure and high temperatures, such as the density (Ai and Lange, 2007; Lange, 1997; Lange and Carmichael, 1987), thermal expensivity (Lange, 1997; Lange and Carmichael, 1987), bulk modulus (Ai and Lange, 2007; Lange and Carmichael, 1987) , heat capacity (Lange and Navrotsky, 1992; Stebbins et al., 1984), and equation of state (Rigden et al., 1984; Rigden et al., 1988; Rigden et al., 1989). The diopside melting curve has been measured experimentally up to 18 GPa (Gasparik, 1996; Scarfe and Takahashi, 1986); the dT/dP melting slope is found to vanish near 17 GPa, requiring a liquid-crystal density inversion (Ai and Lange, 2007). Diffusivity and viscosity were investigated up to 2300 K and 15 GPa (Reid et al., 2001; Reid et al., 2003), and remarkable behavior found: instead of showing a diffusivity maximum at elevated pressure, this relatively unpolymerized liquid, shows a diffusivity minimum near 10 GPa.

Many important questions remain, even at relatively low pressure, including the origin of the melting curve maximum and liquid-crystal density inversion, and the origin of the diffusivity minimum. In the case of experimental studies, dynamic compression of samples pre-heated to the liquid state, has proved fruitful up to a pressure of 40 GPa. But the Hugoniot is known to show a density maximum and it is not clear that such experiments can access the density at the base of the mantle. In Chapter II, to answer these questions, I investigated the structure and equation of state of diopside. The

following properties of diopside liquid are reported: Si-O and Mg-O/Ca-O coordination numbers, Si-O coordination distribution, Mie-Grüneisen equation of state, Grüneisen parameter, heat capacity, and the origin of the liquid–crystal density inversion in the liquid structure.

The dynamics of diopside liquid is investigated in Chapter III. Chemical diffusion controls the rate of chemical reaction of a liquid with its surroundings, and can alter the composition of a liquid on porous flow. Chemical diffusion in silicate liquids shows remarkably rich behavior on increasing pressure. Maxima in the diffusivity at finite pressure are now well known in highly polymerized systems (Angell et al., 1982; Kushiro, 1976). Remarkably, less polymerized compositions, such as diopsde, which are presumably more similar to the composition of deep melts, show exactly the opposite behavior: a minimum in the diffusivity. In this chapter, the self-diffusion coefficients of diopside liquid are investigated up to lower mantle conditions and the contributions of 5-fold coordinated Mg and Si to the diffusivity minimum are discussed.

Chapter IV presents the thermodynamic properties of wollastonite liquid ($CaSiO_3$) and discusses the mixing of $MgSiO_3$-$CaSiO_3$ join. The high-pressure phase of $CaSiO_3$, Ca-perovskite, has been thought to be one of the most important phases in the lower mantle and has been investigated by many experimental studies (Shim et al., 2000; Shim et al., 2002) and computational simulations (Adams and Oganov, 2006; Caracas and Wentzcovitch, 2005; Jung and Oganov, 2005; Li et al., 2006a; Li et al., 2006b; Stixrude et al., 1996; Stixrude et al., 2007; Zhang et al., 2006). However, the physical properties of $CaSiO_3$ liquid at high pressure are still unknown. The $MgSiO_3$-$CaSiO_3$ join represents an ideal system for an exploration of the still unknown thermodynamics of mixing of silicate

melts at high pressure. This system accounts for more 90 % of the bulk silicate Earth and includes diopside, a major component of model basalt compositions. The system is homovalent, and its subsolidus mixing properties are well characterized. In this chapter, we predict the structure and the equation of state of $CaSiO_3$ liquid at high pressure and compare our results with existing lower pressure and lower temperature experiments (Ai and Lange, 2007; Funamori et al., 2004; Lange, 1997; Lange and Carmichael, 1987; Lange and Navrotsky, 1992; Stebbins et al., 1984). The following properties of $CaSiO_3$ liquid were studied: Si-O and Ca-O coordination numbers, Si-O coordination distribution, Mie-Grüneisen equation of state, Grüneisen parameter, heat capacity, and bulk modulus. To understand the mixing of $MgSiO_3$-$CaSiO_3$ join, the volume of mixture is computed by combining my results with previous results on $MgSiO_3$ composition (Stixrude and Karki, 2005).

In this thesis, Chapter II, III, and IV will be submitted for publications. Citations are as follows:

Ni Sun, Lars P. Stixrude, and Bijaya B. Karki, High pressure structure and equation of state of diopside ($CaMgSi_2O_6$) liquid, *to be submitted to Earth and Planetary Science Letters*, 2008a.

Ni Sun, Lars P. Stixrude, and Bijaya B. Karki, Dynamics of diopside liquid at high pressures, *to be submitted*, 2008b.

Ni Sun, Lars P. Stixrude, and Bijaya B. Karki, Thermodynamics of $CaSiO_3$ liquid and mixing on the $MgSiO_3$ - $CaSiO_3$ join, *to be submitted*, 2008c.

References

Adams, D.J. and Oganov, A.R., 2006. *Ab initio* molecular dynamics study of $CaSiO_3$ perovskite at P-T conditions of Earth's lower mantle. Physical Review B, 73: 1841006.

Ai, Y. and Lange, R.A., 2007. The compressibility of CaO-MgO-Al_2O_3-SiO_2 liquids from new acoustic velocity measurements: reevaluation of the equation of state of $CaMgSi_2O_6$-$CaAl_2Si_2O_8$ liquids to 25 GPa. Journal of Geophysical Research, In Press.

Angell, C.A., Cheeseman, P.A. and Tamaddon, S., 1982. Pressure enhancement of ion mobilities in liquid silicates from computer simulation studies to 800 kilobars. Science, 218: 885-887.

Benz, W., Slattery, W.L. and Cameron, A.G.W., 1986. The origin of the Moon and the single-impact hypothesis I. Icarus, 66: 515-535.

Canup, R.M. and Asphaug, E., 2001. Origin of the Moon in a giant impact near the end of the Earth's formation. Nature, 412(6848): 708-712.

Caracas, R. and Wentzcovitch, R., 2005. $CaSiO_3$ perovskite at lower mantle pressures. Geophysical Research Letters, 32: 1029.

de Koker, N., Stixrude, L. and Karki, B.B., 2008. Thermodynamics, structure, dynamics, and freezing of Mg_2SiO_4 liquid at high pressure. Geochimica et Cosmochimica Acta, in press.

Funamori, N., Yamamoto, S., Yagi, T. and Kikegawa, T., 2004. Exploratory studies of silicate melt structure at high pressures and temperatures by in situ X-ray diffraction. Journal of Geophysical Research, 109: B03203.

Gasparik, T., 1996. Melting experiments on the enstatite-diopside join at 70-224 kbar, including the melting of diopside. Contributions to Mineralogy and Petrology, 124: 139-153.

Haggerty, S.E. and Sautter, V., 1990. Ultradeep (greater than 300 kilometers), ultramafic upper mantle xenoliths. Science, 248: 993-996.

Herzberg, C., 1995. Generation of plume magma through time: an experimaental perspective. Chemical Geology, 126: 1-16.

Jung, D.Y. and Oganov, A.R., 2005. *Ab initio* study of the high-pressure behavior of $CaSiO_3$ perovskite. Physics and Chemistry of Minerals, 32: 146-153.

Kushiro, I., 1976. Changes in viscosity and structure of melt of $NaAlSi_2O_6$ composition at high-pressures. Journal of Geophysical Research, 81(35): 6347-6350.

Lange, R.A., 1997. A revised model for the density and thermal expansivity of K_2O-Na_2O-CaO-MgO-Al_2O_3-SiO_2 liquids from 700 to 1900 K: extension to crustal magmatic temperatures. Contributions to Mineralogy and Petrology, 130: 1-11.

Lange, R.A. and Carmichael, I.S.E., 1987. Densities of Na_2O-K_2O-MgO-FeO-Fe_2O_3-Al_2O_3-TiO_2-SiO_2 liquids – new measurements and derived partial molar properties. Geochimica et Cosmochimica Acta, 51: 2931-2946.

Lange, R.A. and Navrotsky, A., 1992. Heat capacities of Fe_2O_3-bearing silicate liquids. Contributions to Mineralogy and Petrology, 110: 311-320.

Li, L. et al., 2006a. Elasticity of $CaSiO_3$ perovskite at high pressure and high temperature. 155: 249-259.

Li, L. et al., 2006b. Phase stability of $CaSiO_3$ perovskite at high pressure and temperature: Insights from as initio molecular dynamics. Physics of the Earth and Planetary Interiors, 155: 260-268.

Miller, G.H., Stolper, E.M. and Ahrens, T.J., 1991. The equation of state of a molten komatiite 2: Application to komatiite petrogenesis and the hadean mantle. Journal of Geophysical Research, 96(B7): 11,849-11,864.

Reid, J.E., Poe, B.T., Rubie, D.C., Zotov, N. and Wiedenbeck, M., 2001. The self-diffusion of silicon and oxygen in diopside ($CaMgSi_2O_6$) liquid up to 15 GPa. Chemical Geology, 174: 77-86.

Reid, J.E. et al., 2003. The viscosity of $CaMgSi_2O_6$ liquid at pressures up to 13 GPa Physics of the Earth and Planetary interiors, 139: 45-54.

Rigden, S.M., Ahrens, T.J. and Stolper, E.M., 1984. Densities of liquid silicates at high-pressures. Sciences, 226: 1071-1074.

Rigden, S.M., Ahrens, T.J. and Stolper, E.M., 1988. Shock compression of molten silicate – results for a model basaltic composition. Journal of Geophysical Research – Solid Earth and Planets, 93: 367-382.

Rigden, S.M., Ahrens, T.J. and Stolper, E.M., 1989. High pressure equation of state of molten anorthite and diopside. Journal of Geophysical Research, 94: 9508-9522.

Scarfe, C.M. and Takahashi, E., 1986. Melting of garnet peridotite to 13 GPa and the early history of the upper mantle. Nature, 322: 354-356.

Shim, S.-H., Duffy, T.S. and Shen, G., 2000. The equation of state of $CaSiO_3$ perovskite to 108 GPa at 300 K. Physics of the Earth and Planetary Interiors, 120: 327-338.

Shim, S.-H., Jeanloz, R. and Duffy, T.S., 2002. Tetragonal Structure of $CaSiO_3$ perovskite above 20 GPa. Geophysical Research Letters, 29(24): 2166.

Stebbins, J.F., Carmichael, I.S.E. and Moret, L.K., 1984. Heat Capacities and entropies of silicate liquids and glasses. Contribution to Mineralogy and Petrology, 86: 131-148.

Stixrude, L., Cohen, R.E., Yu, R. and Karkauer, H., 1996. Prediction of phase transition in $CaSiO_3$ perovskite and implications for lower mantle structure. American Mineralogist, 81: 1293-1296.

Stixrude, L. and Karki, B., 2005. Structure and freezing of $MgSiO_3$ liquid in Earth's lower mantle. Science 310: 297-299.

Stixrude, L., Lithgow-Bertelloni, C., Kiefer, B. and Fumagalli, P., 2007. Phase stability and shear softening in $CaSiO_3$ perovskite at high pressure. Physical Review B, 75: 024108.

Zhang, Y., Zhao, D., Matsui, M. and Guo, G., 2006. Equation of state of $CaSiO_3$ perovskite: a molecular dynamics study. Physics and Chemistry of Minerals, 33: 126-137.

CHAPTER II

HIGH PRESSURE STRUCTURE AND EQUATION OF STATE OF DIOPSIDE LIQUID

2.1 Abstract

$CaMgSi_2O_6$ liquid has been investigated over the entire mantle pressure regime using first principles molecular dynamics simulations with density functional theory in the local density approximation and the ultra-soft plane-wave pseudopotential method. The equilibrated liquid structure is much more densely packed at high pressure. The average Si-O coordination number increases nearly linearly from 4 to 6 with compression. Our results are well fitted by Mie-Grüneisen equation of state, $P(V,T) = P_C(V,T_0) + P_{TH}(V,T)$, with a Grüneisen parameter that linearly increases and heat capacity that linearly decreases with compression. The liquid becomes denser than coexisting diopside at 14±1 GPa. The liquid-crystal density inversion originates in liquid structure, which shows cation-oxygen coordination numbers that exceed those of diopside at the crossover.

2.2 Introduction

The knowledge of silicate liquids over the large range of pressure and temperature in Earth's mantle is important to understand magma generation and transport, as well as the chemical and thermal evolution of Earth. Although it is well known that most of the present-day mantle is solid, there is increasing evidence for the importance of liquids even below the shallow upper mantle where most magma is generated. Evidence from xenoliths (some thought to come from depths of 300-400 km) (Haggerty and Sautter, 1990), the origin of komatiites (thought to originate at depths of 500-670 km or even in the lower mantle) (Herzberg, 1995; Miller et al., 1991), seismic observations of ultra low velocity zone (ULVZ) at the core mantle boundary (136 GPa, 2890 km depth) (Garnero and Helmberger, 1995; Mori and Helmberger, 1995; Revenaugh and Meyer, 1997), and giant-impact models of lunar formation (Benz et al., 1986; Canup and Asphaug, 2001), which predict a largely or completely molten early Earth, all emphasize the need to understand the physics of silicate liquids over the entire mantle pressure regime.

Diopside ($CaMgSi_2O_6$) liquid is a major component of basalt; its high-pressure end members, Mg-perovskite ($MgSiO_3$) and Ca-perovskite ($CaSiO_3$), make up more than 80% of the lower mantle. Diopside liquid has been studied extensively in the lab at ambient pressure where its thermodynamic properties are well characterized, including the density (Ai and Lange, 2007; Lange, 1997; Lange and Carmichael, 1987), thermal expansivity (Lange, 1997; Lange and Carmichael, 1987), bulk modulus (Ai and Lange, 2007; Lange and Carmichael, 1987) , and heat capacity (Lange and Navrotsky, 1992; Stebbins et al., 1984). The equation of state of diopside liquid has been studied by shock

wave experiments up to 40 GPa (Rigden et al., 1989). The diopside melting curve has been measured up to 18 GPa (Gasparik, 1996; Scarfe and Takahashi, 1986). Previous molecular dynamics simulations of diopside liquid provided high-pressure results and showed structure, bulk moduli, and thermal expansivity of diopside liquid up to 5 GPa (Matsui, 1996).

Important questions remain. Diopside is perhaps the simplest system to exhibit liquid-crystal density inversion: the liquid becomes denser than the coexisting solid along the melting line near 17 GPa (Ai and Lange, 2007). Although the phenomenon of liquid-crystal density inversion has profound geophysical and geochemical implications (Stolper et al., 1981), the origin of this behavior, presumably related to pressure-induced changes in liquid structure, is not understood even in the diopside system. The properties of diopside melt are unknown above 40 GPa, leaving most of the pressure regime of Earth's mantle (up to 136 GPa) unexplored. It has been proposed on the basis of studies of $MgSiO_3$ liquid that silicate melts show a Grüneisen parameter that increases on compression, behavior opposite to that of crystalline silicates, that may have important implications for the initial thermal state of Earth (Stixrude and Karki, 2005). Whether this behavior is exhibited by diopside liquid is unknown.

In this study, we investigated diopside liquid across the entire mantle pressure-temperature regime by first principles molecular dynamics (FPMD) simulations, which have been successfully used to study silicate liquid (Stixrude and Karki, 2005) and which allow us to predict physical properties at high temperature and pressure. Our goals are to investigate the structure, equation of state, and thermodynamic properties of diopside

liquid over the whole mantle pressure regime and to compare with experiment and the properties of crystalline assemblages.

2.3 Computational Methods

Our simulations are based on density functional theory (DFT) (Kohn and Sham, 1965) in the local density approximation (LDA) and the ultra-soft plane-wave pseudopotential method. The calculations were performed with the Vienna ab initio simulation package (VASP) (Kresse and Furthmüller, 1996a; Kresse and Furthmüller, 1996b; Kresse and Hafner, 1993). We computed the electronic structure and forces at the Brillouin zone center with an energy cutoff, E_{cut}=400 eV.

All simulations in this study were performed for an 80 atom primary simulation cell of cubic shape in the canonical ensemble using the thermostate of Nosé (Nosé, 1984) for an 80-atom cubic unit cell. The initial condition is a pyroxene supercell homogeneously strained to a cubic shape. The system is melted at 6000 K, then isochorically cooled to 4000 K and 3000K. For each calculation, the total run duration is 8 ps, the last 6.4 ps are used to compute equilibrium properties. Convergence tests, including larger systems (160 atoms) and longer runs (11 ps), produced results within the statistical uncertainty of our simulations. The volumes we explored range from 81.8 cm^3/mol, the volume of the liquid at the ambient pressure fusion point (Lange and Carmichael, 1987) to 38.9 cm^3/mol, at which the pressure is beyond that of the core-mantle boundary. We report volumes as V/V_X, where V_x=77.8 cm^3/mol is the experimental volume of enstatite composition ($Mg_2Si_2O_6$) liquid at the ambient-pressure

melting point, 1830K (Lange and Carmichael, 1987), and a convenient reference to compare with our previous studies of $MgSiO_3$.

We further ensured a liquid state by inspection of the radial distribution functions and the mean squared displacement with time. These tests showed that all simulations resulted in a liquid state except for $V=V_x/2$ and 3000K, which showed no significant diffusion and is considered to be a glass within the resolution of our simulations. This point is excluded from our analysis of thermodynamic properties.

We apply the following corrections to the simulated pressure

$$P(V,T) = P_{MD}(V,T) + P_{Pulay}(V) + P_{emp} \quad (1)$$

where P_{MD} is the simulated pressure, P_{Pulay} is the Pulay (finite basis-set) correction (Francis and Payne, 1990) and P_{emp} is an empirical correction. The correction terms are computed at static conditions with a 20 atom cell of crystalline diopside fully relaxed to the equilibrium structure and a 2x2x2 Monkhorst-Pack k-point mesh. The Pulay correction is given by

$$P_{Pulay}(V) = P\left(V; E_{cut} = 600eV\right) - P\left(V; E_{cut} = 400eV\right) \quad (2)$$

and is found to vary nearly linearly with volume from 2.55 GPa at $V=V_x$ to 4.69 GPa at $V=V_x/2$. The empirical term corrects for the well known and systematic tendency towards over-binding in the local density approximation (Karki et al., 2001; Oganov et al., 2001)

$$P_{emp} = -P_{LDA}\left(V_{static}\right) \quad (3)$$

where V_{static} is the experimental volume of diopside at ambient pressure and static conditions. The value of V_{static} was approximated via the semi-empirical thermodynamic model of (Stixrude and Lithgow-Bertelloni, 2005) and produced a value 0.74 % less than the volume of diopside at ambient conditions. The fully converged value of P_{LDA} is

computed at this volume with an energy cutoff of 600 eV. The value obtained P_{emp}=2.46 GPa, is consistent with the well-known over-binding tendency of LDA.

Liquid structure is examined via the radial distribution function $g(r)$ (McQuarrie, 1976). Coordination environments are characterized by the bond length

$$\bar{r}_{\alpha\beta} = \frac{\int_0^{r_{\min}} r g_{\alpha\beta}(r) dr}{\int_0^{r_{\min}} g_{\alpha\beta}(r) dr} \tag{4}$$

and the coordination number

$$C_{\alpha\beta} = 4\pi\rho_\beta \int_0^{r_{\min}} r^2 g_{\alpha\beta}(r) dr \tag{5}$$

where $g_{\alpha\beta}$ is the partial radial distribution function for atom types α and β, r is the distance, r_{min} is the distance at the first minimum in $g_{\alpha\beta}$, and ρ_β is the number atoms of type β per unit volume.

2.4 Results

2.4.1 Structure

Results are shown in Table 2.1. The liquid structure changes substantially on compression (Figure 2.1). At $V=V_x$, the liquid shows an average Si-O coordination number of 4, the same as the solidus crystalline phase at this volume (diopside), and an average Si-O coordination number of 6 at $V=V_x/2$ (Figure 2.2a). The coordination number increases nearly linearly with compression from $V=V_x$ to $V=V_x/2$ and does not appear to depend systematically on temperature. These results are essentially identical to those

found previously for $Mg_2Si_2O_6$ liquid (Stixrude and Karki, 2005). The increase of Si-O coordination number is also observed in silicate glass (Stebbins and McMillan, 1989; Xue et al., 1989). Between $V=V_x$ and $V=1.05V_x$, the coordination number shows a different dependency on volume and changes very little, from 4.08 to 4.06. The average cation coordination numbers of $CaMgSi_2O_6$ liquid that we find are consistent with previous experimental studies at ambient pressure (Table 2.2).

The increase of average Mg-O and Ca-O coordination numbers with compression is also observed and does not depend significantly on temperature (Figure 2.2b). The increase of the mean Mg-O coordination number of $CaMgSi_2O_6$ liquid is essentially identical with that in $Mg_2Si_2O_6$ liquid and varies from 5.2 at $V=1.05V_X$ to 7.9 at $V=V_X/2$. The mean Ca-O coordination number is larger than Mg-O, consistent with expectations based on the larger ionic radius and varies from 6.0 at $V=1.05V_X$ to 9.8 at $V=V_X/2$. The O-O coordination number initially increases on compression, and then decreases with compression when the volume is smaller than $0.7V_X$. The origin of the decrease in O-O coordination number on compression at large compressions can be seen in the O-O radial distribution function. At large compressions, the first peak in g_{OO} splits and a small secondary peak appears near 3 Å (Figure 2.3).

We also investigated the Si-O coordination number distribution at different temperatures (Figure 2.4). On compression, the fraction of 3-fold and 4-fold coordinated Si atoms decreases monotonically and the fraction of 6-fold, and 7-fold coordinated Si atoms increases monotonically. The fraction of 5-fold coordinated Si atoms initially increases on compression and then decreases, reaching a maximum value at V/V_X=0.7-0.8, where the pressure is 14-34 GPa at 3000 K. With increasing temperature, the variety

of Si-O coordination environments increases. For example, at $V=V_x$, the proportion of 3-fold and 5-fold coordination increases with increasing temperature at the expense of 4-fold.

2.4.2 Equation of State

Results are shown in Table 2.1. We find that the equation of state (Figure 2.5a) is well described by the Mie-Grüneisen equation

$$P(V,T) = P_C(V,T_C) + P_{TH}(V,T) \tag{6}$$

where P_C is pressure at the reference temperature T_C (T_C = 3000 K in this study), and $P_{TH}(V,T)$ is the thermal pressure. The equation of state of diopside liquid at T_C is described by the third-order Birch-Murnaghan equation (Birch, 1986) with zero pressure volume, bulk modulus, and first pressure derivative of the bulk modulus: V_0=1.24V_x, K_0= 9.74 GPa, and K_0'=6.82. We find that the thermal pressure is linear in temperature over the studied volume range to within the resolution of our simulations,

$$P_{TH}(V,T) = \frac{\gamma(V)}{V} C_V(V)(T - T_C) \tag{7}$$

where γ is Grüneisen parameter and C_V is isochoric heat capacity. The Grüneisen parameter γ is shown in Figure 2.5b, and is calculated at each volume from the identity

$$\gamma \equiv V\left(\frac{\partial P}{\partial E}\right)_V \tag{8}$$

where E is the internal energy. C_V is computed from

$$C_V = \left(\frac{\partial E}{\partial T}\right)_V \tag{9}$$

The internal energy is also found to vary linearly with temperature along isochores to within the resolution of our simulations. The values of the Grüneisen parameter and the heat capacity are then determined from the slopes.

The variation of C_V on compression is shown in Figure 2.5c: from 4.78 ± 0.07 *Nk* at $V=1.05V_x$ (the experimental values are 4.146 ± 0.085 *Nk* (Lange and Navrotsky, 1992), and 4.08 ± 0.06 *Nk* (Stebbins et al., 1984)), then decreasing nearly linearly to 4.13 ± 0.15 *Nk* at $V=V_x/2$, where *N* is the number of atoms and *k* is the Boltzmann constant. The Grüneisen parameter γ is 0.47 ± 0.14 at $V=1.05V_x$ (the experimental value is 0.464 ± 0.026, calculated from (Ai and Lange, 2007; Lange, 1997; Lange and Navrotsky, 1992)) and increases to 1.14 ± 0.13 at $V = V_x/2$. The increase of the Grüneisen parameter with compression is large (factor of two over two-fold compression) but somewhat smaller than the increase found previously in $Mg_2Si_2O_6$ liquid over the same range (Stixrude and Karki, 2005) (factor of three). The variation of the Grüneisen parameter and the heat capacity are accurately described by

$$\gamma(V) = \gamma_X + \gamma'(V/V_X - 1) \tag{10}$$

$$C_V(V) = C_{VX} + C'_V(V/V_X - 1) \tag{11}$$

With $\gamma_X = 0.51$, $\gamma' = -1.31$, $C_{VX} = 4.68$, and $C'_V = 1.07$.

Because our simulations are in the canonical ensemble, the most direct way to compare with experiments is at the volume found experimentally at ambient pressure fusion (81.8 cm3/mol or $V/V_x=1.05$) (Figure 2.5a). We compare our simulated pressure on this isochore, to that constrained experimentally via the relationin

$$\left(\frac{\partial P}{\partial T}\right)_V = \alpha K_T \tag{12}$$

where the experimental slope is computed from measured values of the thermal

expansivity α (Lange, 1997) and the isothermal bulk modulus K_T (Ai and Lange, 2007). We may compare the experimental value of the slope (2.2 ± 0.1 MPa/K) to that found directly from our simulations by the variation of the pressure along the isochore (1.95 ± 0.1 MPa/K).

In order to compare with experimental shock wave studies (Rigden et al., 1989), we computed the Hugoniot of $CaMgSi_2O_6$ liquid (Figure 2.6). The Hugoniot is found as the set of state points that satisfy the Rankine - Hugoniot equation,

$$E_H - E_0 = \frac{1}{2}(V_0 - V)P_H \tag{13}$$

where E_H and P_H are the internal energy and pressure on the Hugoniot; and E_0 and V_0 are internal energy and volume at ambient pressure and the pre-shocked temperature. E_H and P_H are computed from our molecular dynamics simulations and solutions to the equation are found via interpolation. The computed Hugoniot at pressures beyond those that have been measured experimentally are a prediction that could be tested with further shock wave studies.

We compare the density of diopside liquid from our calculations to that of crystalline diopside (Stixrude and Lithgow-Bertelloni, 2005) at a temperature similar to that of the maximum melting temperature (2400 K) (Figure 2.7). We find that the density of the liquid exceeds that of the crystal at 14±1 GPa, where the density is 3.5 g/cm^3. The Si-O coordination number of the liquid at this point is 4.7, substantially greater than that of the crystal. The pressure at which the density crossover occurs increases slightly with decreasing temperature, consistent with the results of Ai and Lange (2007) who found that diopside and (metastable) liquid have the same density at 17 GPa and 1900 K.

2.5 Discussions

The diopside liquid structure near ambient pressure differs substantially from that of crystalline diopside. The crystal structure consists of infinite chains of corner-linked SiO_4 tetrahedra, bonded to MgO_6 octahedra and CaO_8 dodecahedra. At V/V_X=1, the liquid has predominantly 4-fold coordinated silicons but also a significant number of 3-fold, and 5-fold, with the proportion of these odd coordination environments increasing with increasing temperature. The infinite chain structure is absent in the liquid (Figure 2.1). The Mg-O and Ca-O coordination numbers in the liquid (4.9 and 5.9, respectively at V=1.05V_x and 3000 K) are substantially less than that of the crystal (6 and 8 respectively), which accounts for the volume of fusion.

An increase in the average Si-O coordination number with increasing pressure accounts for the greater compressibility of the liquid as compared with the solid and for liquid-crystal density inversion near 14±1 GPa at 2400 K. The Si-O, Mg-O and Ca-O coordination numbers in the liquid (4.7, 6.7 and 8.5, respectively at V=0.8V_x) all exceed those of the crystal at 14 GPa. The liquid-crystal density inversion is linked to the experimentally observed melting curve maximum (Gasparik, 1996; Ai and Lange, 2007) via the Claussius-Clapeyron relation

$$\left(\frac{\partial T}{\partial P}\right)_{eq} = \frac{\Delta V}{\Delta S} \tag{14}$$

so that when the volume (density) contrast, ΔV vanishes, the melting slope also vanishes and is negative at higher pressures. At pressures slightly higher than the liquid-crystal density inversion, the solid phase transforms to a mixture of $CaSiO_3$ perovksite and garnet-majorite, in which Si is in 6-fold (perovksite) and 4- and 6-fold (garnet)

coordination. The liquid can be viewed as anticipating the Si-O coordination increase that occurs at higher pressure in the solid state. This behavior is very similar to that of many alkali halides that show the cation-anion coordination number and the density of the liquid exceeding that of the B1 phase at pressures slightly lower than that of the B1-B2 solid-solid phase transition (Ross and Rogers, 1985; Tallon, 1979).

The increase of the Grüneisen parameter of diopside liquid with compression may have important implications for the initial thermal state of Earth. This behavior is opposite to that of all mantle crystalline phases, for which the Grüneisen parameter universally decreases on compression (Stixrude and Lithgow-Bertelloni, 2005). Previous analyses of pre-heated shock wave experiments have assumed that the Grüneisen parameter decreases on compression. We have also found that the Grüneisen parameter increases on compression in Mg_2SiO_4, $MgSiO_3$, and SiO_2 composition liquids (de Koker et al., 2008; Karki et al., 2007; Stixrude and Karki, 2005). A recent shock wave experimental study also finds that γ increases on compression in Mg_2SiO_4 liquid (Mosenfelder et al., 2007). The Grüneisen parameter is geophysically significant because it controls the adiabatic gradient

$$\left(\frac{\partial \ln T}{\partial P}\right)_S = \frac{\gamma}{K_S} \tag{15}$$

where K_S is the adiabatic bulk modulus. The fact that γ in the silicate liquid is much greater at high pressure than previously thought means that the adiabatic gradient in an initial magma ocean, and the temperature at depth in such an ocean, will be much greater than previously thought.

Our simulations show that pre-heated shock wave experiments on initially molten samples should provide meaningful constraints on the equation of state at the pressure-

temperature conditions at the base of the mantle. In particular, we find no density maximum along the Hugoniot over the entire mantle pressure regime (Figure 2.6). We find that the density on the Hugoniot at 136 GPa, where T_H=9000 K, is 5 g/cm^3, only 7 % less than the density at 4000 K, the expected temperature at the core-mantle boundary (Alfe et al., 2002; Boehler, 2000).

2.6 Conclusions

We have successfully investigated $CaMgSi_2O_6$ liquid at lower mantle conditions using first principles molecular dynamics simulations with density functional theory in the local density approximation and the ultra-soft plane-wave pseudopotential method. Our results are consistent with existing experiments. The liquid structure differs significantly from the crystalline phase at low pressure and becomes much more densely packed at high pressure, with the average Si-O coordination number increasing nearly linearly from 4 to 6 with compression. Our results are well fitted by the Mie-Grüneisen equation of state with a Grüneisen parameter that increases rapidly on compression. The liquid becomes denser than coexisting diopside at 14±1 GPa. The liquid-crystal density inversion originates in liquid structure, which shows cation-oxygen coordination numbers that exceed those of diopside at the crossover.

2.7 Acknowledgements

This research was supported by the National Science Foundation under grants EAR-0409074 and EAR-0409121. Computing facilities were provided by CCT at Louisiana State University.

TABLE 2.1 The results of first principles molecular dynamics simulations of $CaMgSi_2O_6$ liquids. Simulation at 3000 K and V/V_x=0.5 apparently produced a glass so that the properties cannot be considered equilibrated. The symbol σ denotes uncertainty. The internal energy and enthalpy are per simulation cell (80 atoms).

T(K)	V/Vx	ρ(g/cm^3)	P(GPa)	σP(GPa)	E(eV)	σE(eV)	H(eV)	σH(eV)
3000	1.05	2.65	3.28	1.43	-564.255	.532	-542.006	9.721
3000	1	2.78	4.94	1.43	-566.129	.528	-534.248	9.218
3000	0.9	3.09	9.00	1.46	-565.925	.918	-513.655	8.526
3000	0.8	3.48	17.53	1.43	-565.036	.603	-474.585	7.393
3000	0.7	3.98	34.49	1.63	-561.059	.273	-405.336	7.382
3000	0.6	4.64	70.04	1.61	-543.143	.538	-272.074	6.251
3000	0.5*	5.57	158.74	1.44	-487.668	.114	24.330	4.641
4000	1.05	2.65	4.73	1.45	-534.475	1.021	-502.386	9.901
4000	1	2.78	7.10	1.43	-534.980	1.522	-489.189	9.346
4000	0.9	3.09	12.19	1.45	-536.852	1.415	-466.078	8.511
4000	0.8	3.48	21.95	1.45	-537.668	.393	-424.377	7.491
4000	0.7	3.98	40.58	1.45	-530.878	.607	-347.636	6.567
4000	0.6	4.64	77.02	1.44	-517.748	.852	-219.639	5.648
4000	0.5	5.57	160.08	1.55	-467.331	1.284	48.971	5.158
6000	1.05	2.65	9.76	1.44	-465.094	1.248	-398.927	9.820
6000	1	2.78	12.42	1.44	-468.763	.902	-388.619	9.319
6000	0.9	3.09	19.06	1.42	-471.402	1.564	-360.752	8.416
6000	0.8	3.48	31.05	1.44	-471.904	1.144	-311.645	7.533
6000	0.7	3.98	52.78	1.43	-468.907	1.276	-230.581	6.589
6000	0.6	4.64	93.98	1.50	-453.892	.964	-90.160	5.899
6000	0.5	5.57	180.12	1.49	-408.592	1.905	172.365	5.166

TABLE 2.2 Comparison of Mg and Ca structure in simulated diopside liquid and experimental data. $r_{Mg\text{-}O}$ is Mg-O bond length, $r_{Ca\text{-}O}$ is Ca-O bond length, $C_{Mg\text{-}O}$ is coordination number of Mg-O, and $C_{Ca\text{-}O}$ is coordination number of Ca-O. FPMD results (this study) are at V/V_X = 1.05 and 3000K (P = 3.19 ± 1.43 GPa) and the experimental results are at ambient pressure. [1]$MgSiO_3$ liquid at 2000K and $CaSiO_3$ liquid at 1900K (Waseda and J.M.Toguri, 1977), [2]CaMg2 liquid at 1700K (Fiske and Stebbins, 1994),and [3]Multiple silicate liquids at 1700K (George and Stebbins, 1998). * 44 mole percent MgO-SiO_2 and 45 mole percent CaO-SiO_2 (Waseda and J.M.Toguri, 1977).

	This study	Experiment
$r_{Mg\text{-}O}$	2.21	2.16[1*], 2.08[2]
$r_{Ca\text{-}O}$	2.50	2.41[1*]
$C_{Mg\text{-}O}$	4.9	4.8[1], 5~7[3]
$C_{Ca\text{-}O}$	5.9	6.6[1],

FIGURE 2.1 $CaMgSi_2O_6$ liquid structure at (a) 3000 K and $V=V_x$ and (b) 3000 K and $V=V_x/2$. In blue are the Si-O polyhedra, in yellow are the Mg ions, and in light blue are the Ca ions. The black solid line indicates the primary simulation cell.

(a)

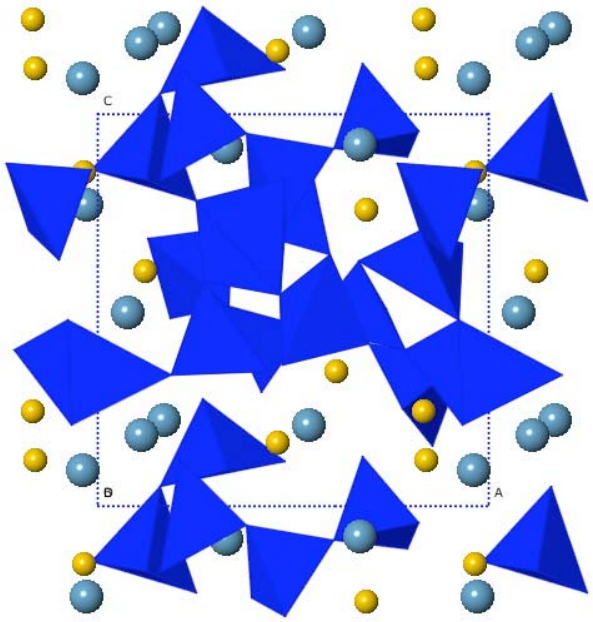

(b)

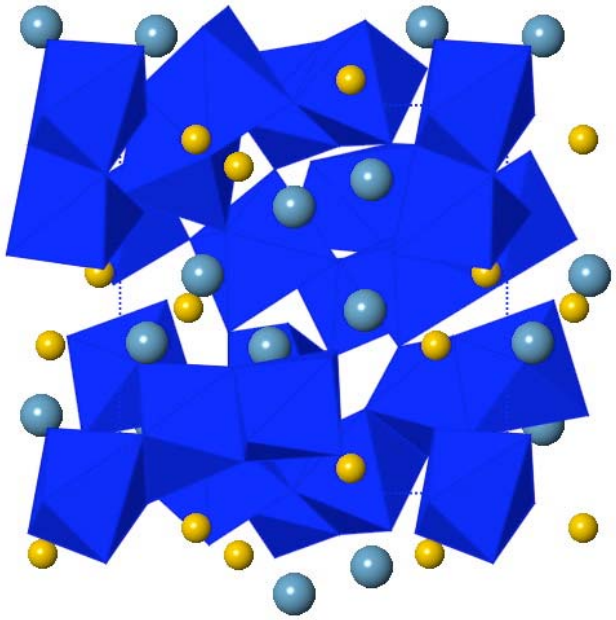

FIGURE 2.2 Mean coordination numbers at 3000 K (blue symbols), 4000 K (green symbols), and 6000 K (red symbols). The dashed lines represent temperature averaged values. We compare to the temperature averaged values of coordination numbers in MgSiO3 liquid from Stixrude and Karki (2005). (a) Si-O (b) Mg-O and Ca-O (c) O-O.

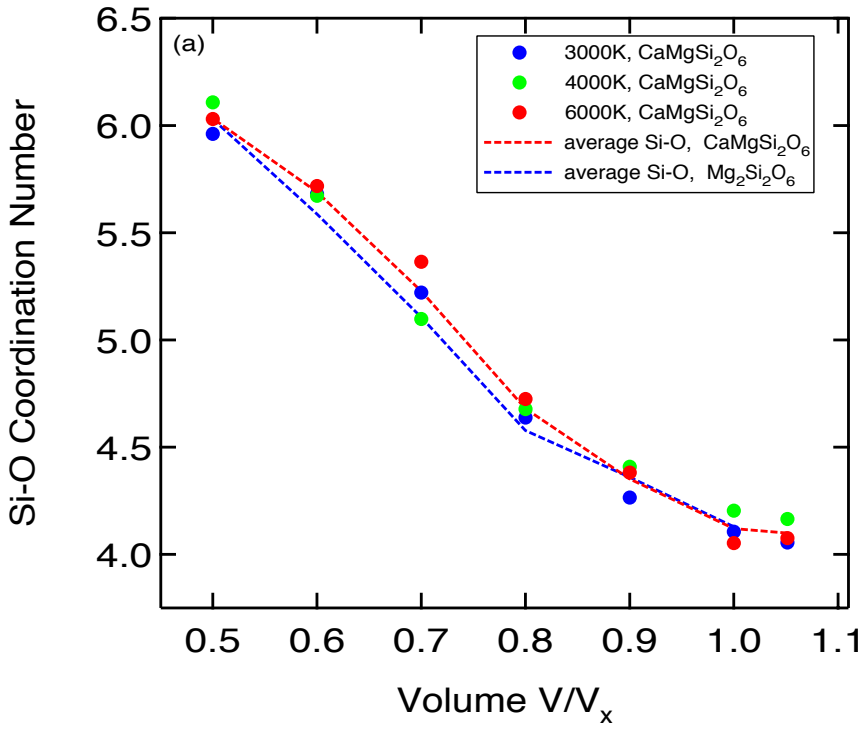

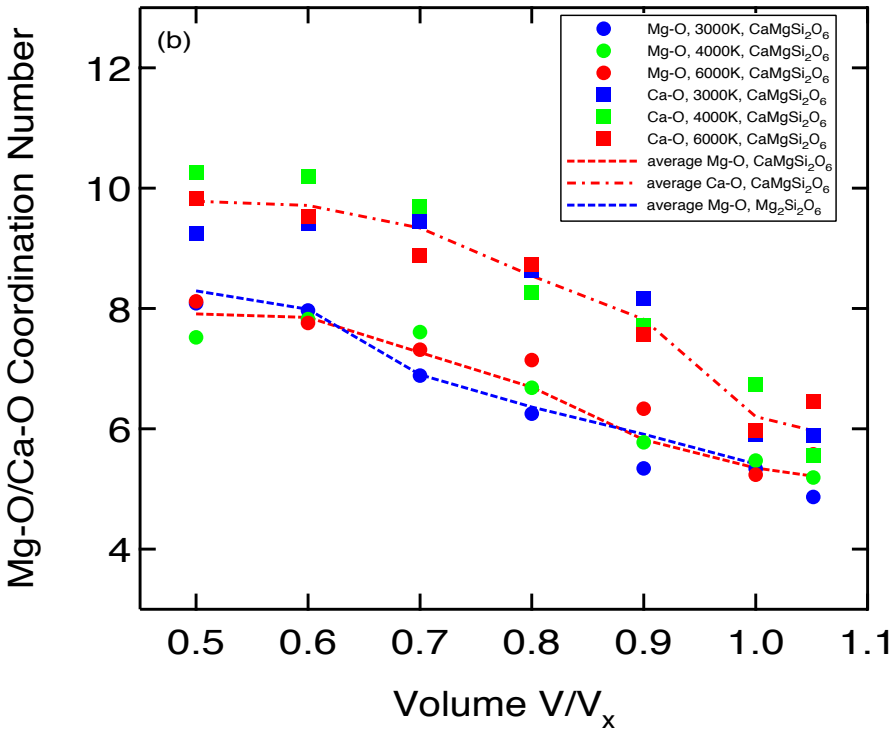
(b)
Mg-O, 3000K, CaMgSi2O6
Mg-O, 4000K, CaMgSi2O6
Mg-O, 6000K, CaMgSi2O6
Ca-O, 3000K, CaMgSi2O6
Ca-O, 4000K, CaMgSi2O6
Ca-O, 6000K, CaMgSi2O6
average Mg-O, CaMgSi2O6
average Ca-O, CaMgSi2O6
average Mg-O, Mg2Si2O6
Mg-O/Ca-O Coordination Number
Volume V/Vx
12
10
8
6
4
0.5
0.6
0.7
0.8
0.9
1.0
1.1

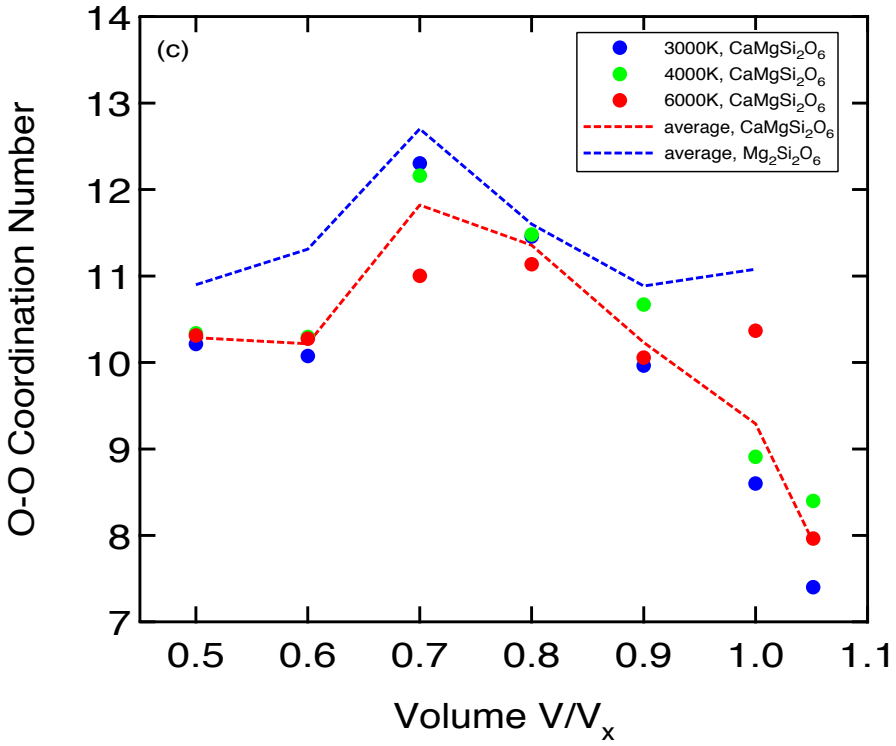
(c)
3000K, CaMgSi2O6
4000K, CaMgSi2O6
6000K, CaMgSi2O6
average, CaMgSi2O6
average, Mg2Si2O6
O-O Coordination Number
Volume V/Vx
14
13
12
11
10
9
8
7
0.5
0.6
0.7
0.8
0.9
1.0
1.1

FIGURE 2.3 Partial radial distribution function of Mg-O, Ca-O, Si-O, and O-O at 3000 K and (a) V=V_x and (b) V=V_x/2.

(a)

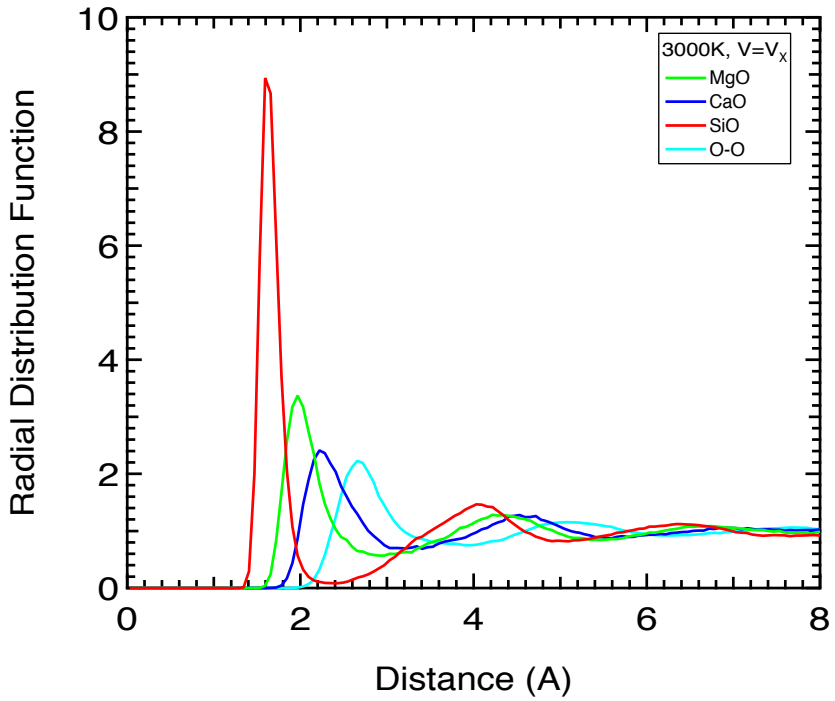

(b)

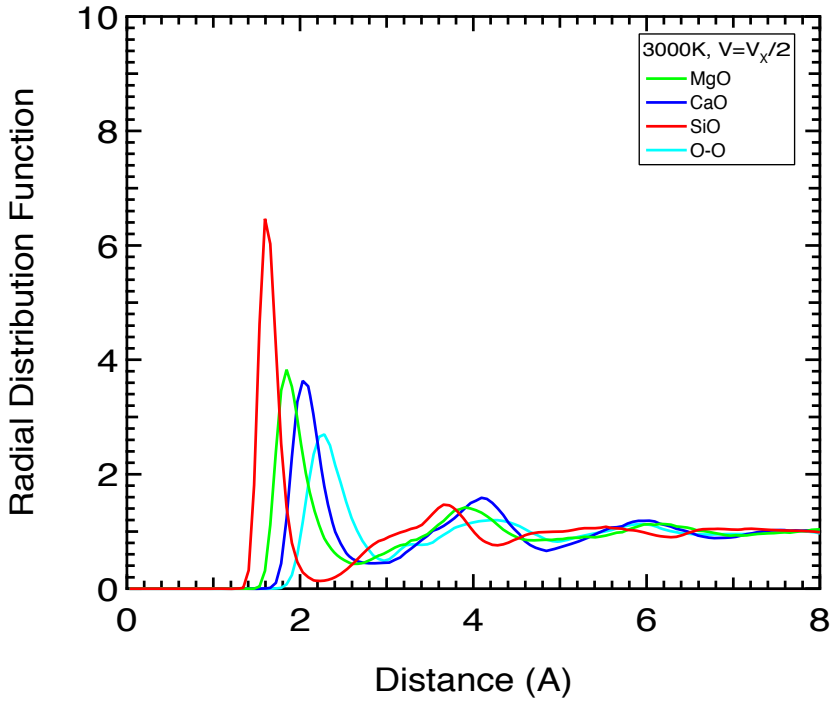

FIGURE 2.4 Si-O coordination distribution in $CaMgSi_2O_6$ liquid at (a) 3000 K (b) 4000 K, and (c) 6000 K. The numbers labeling the lines refer to the coordination number.

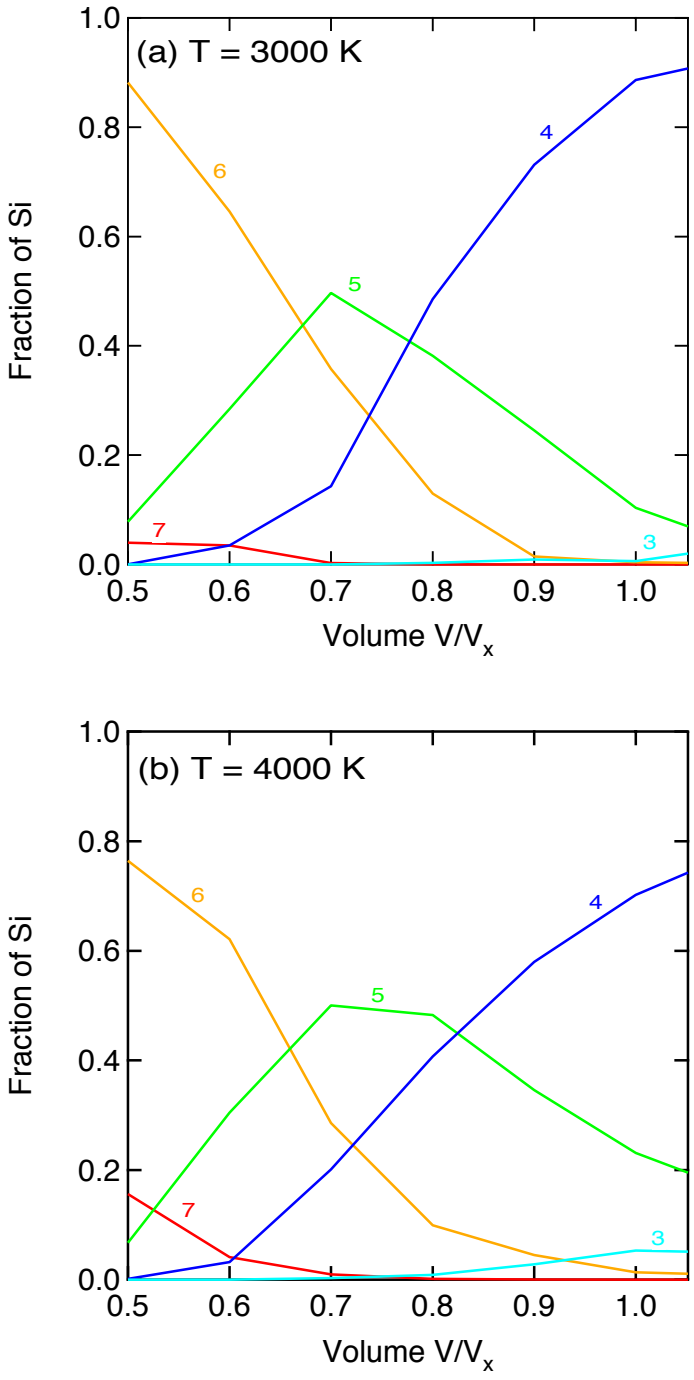

FIGURE 2.4 (continued)

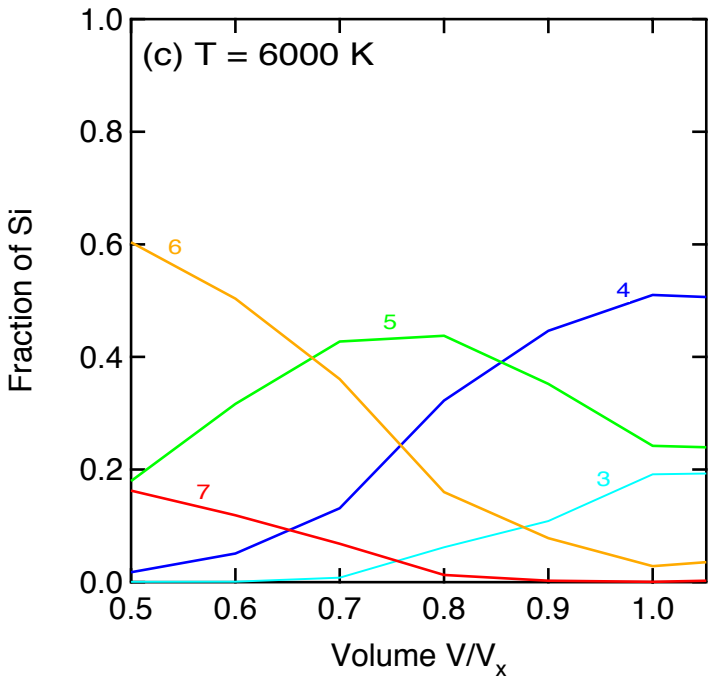

FIGURE 2.5 (a) Equation of state of $CaMgSi_2O_6$ liquid. FPMD results (solid symbols) and Mie-Grüneisen equation of state (curves) fit to the FPMD results at 3000K (blue), 4000 K (green), and 6000 K (red). The uncertainties are within the size of the symbols. The inset is the comparison between simulation results and experimental results at V = 81.8 cm^3/mol, the experimental volume of diopside liquid at the ambient-pressure melting point, 1665K (Lange and Carmichael, 1987). The shading represents the experimental results with uncertainty (Ai and Lange, 2007; Lange, 1997). The open circles are the FPMD results.
(b) Grüneisen parameter, γ, as a function of volume. The circles are the FPMD results and the square is the experimental result, which is calculated from (Ai and Lange, 2007; Lange, 1997; Lange and Navrotsky, 1992). The straight line is fitted by linear regression.
(c) Heat capacity, C_V, as a function of volume. The circles are the FPMD results and the squares are experimental result (Lange and Navrotsky, 1992; Stebbins et al., 1984). The straight line is fitted by linear regression.

(a)

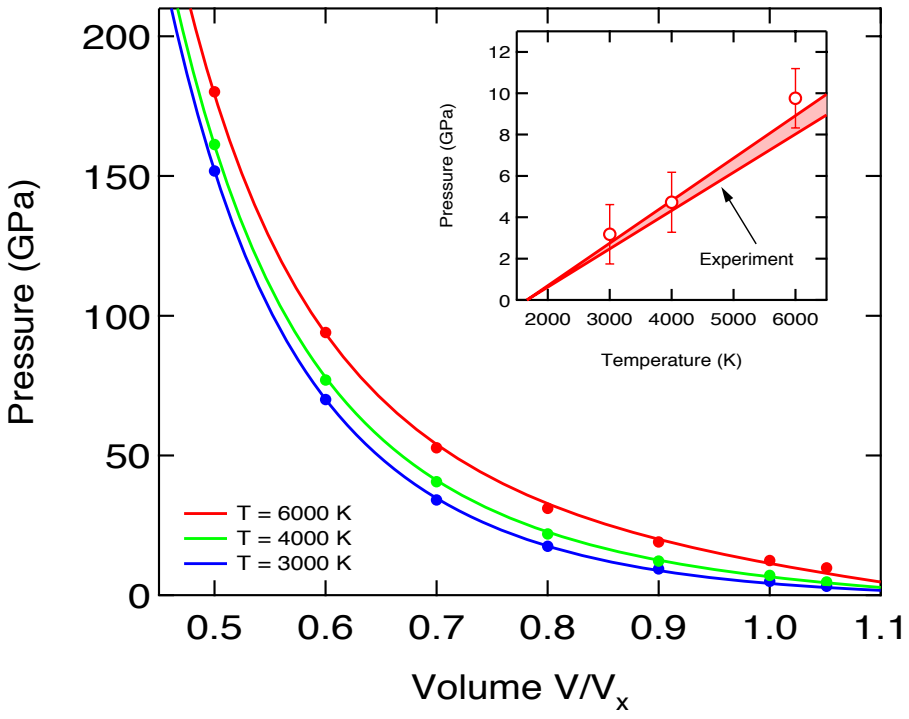

FIGURE 2.5 (continued)

(b)

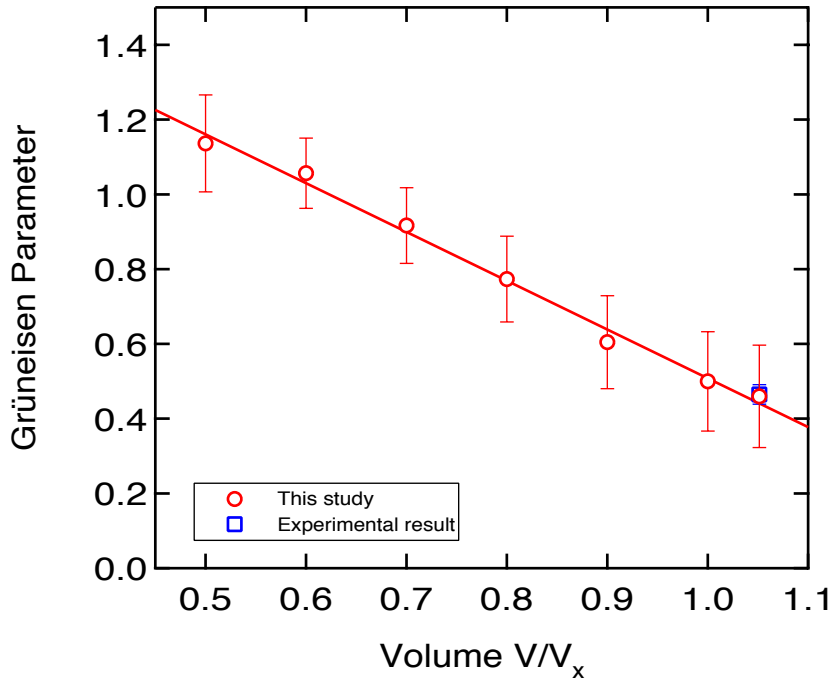

(c)

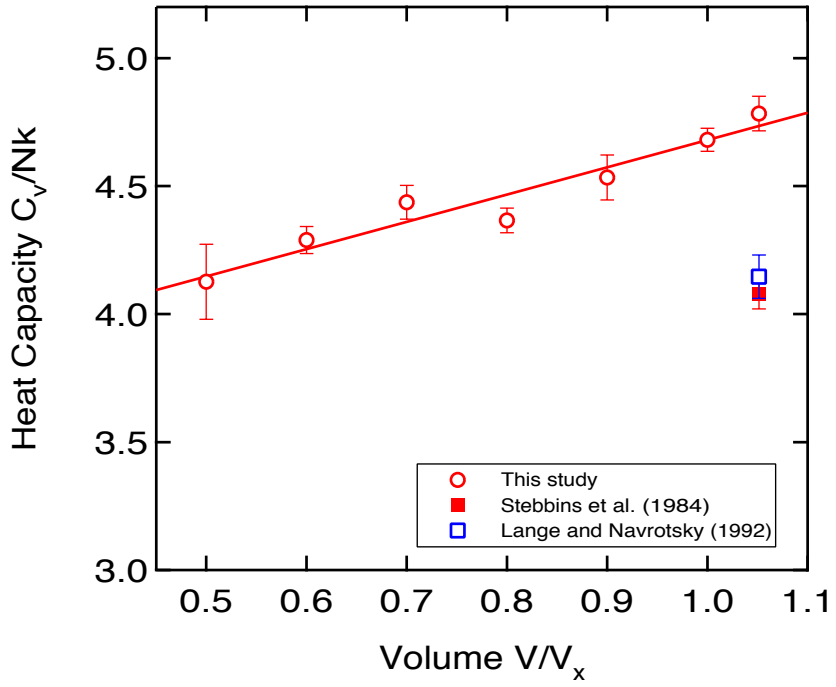

FIGURE 2.6 Hugoniot for $CaMgSi_2O_6$ liquid in the pressure-density plane. The red curve is the calculated Hugoniot and the red open circles are shock wave measurements (Rigden et al., 1989). The blue open circle is from (Lange, 1997). The inset shows calculated Hugoniot density and temperature over a wider pressure interval.

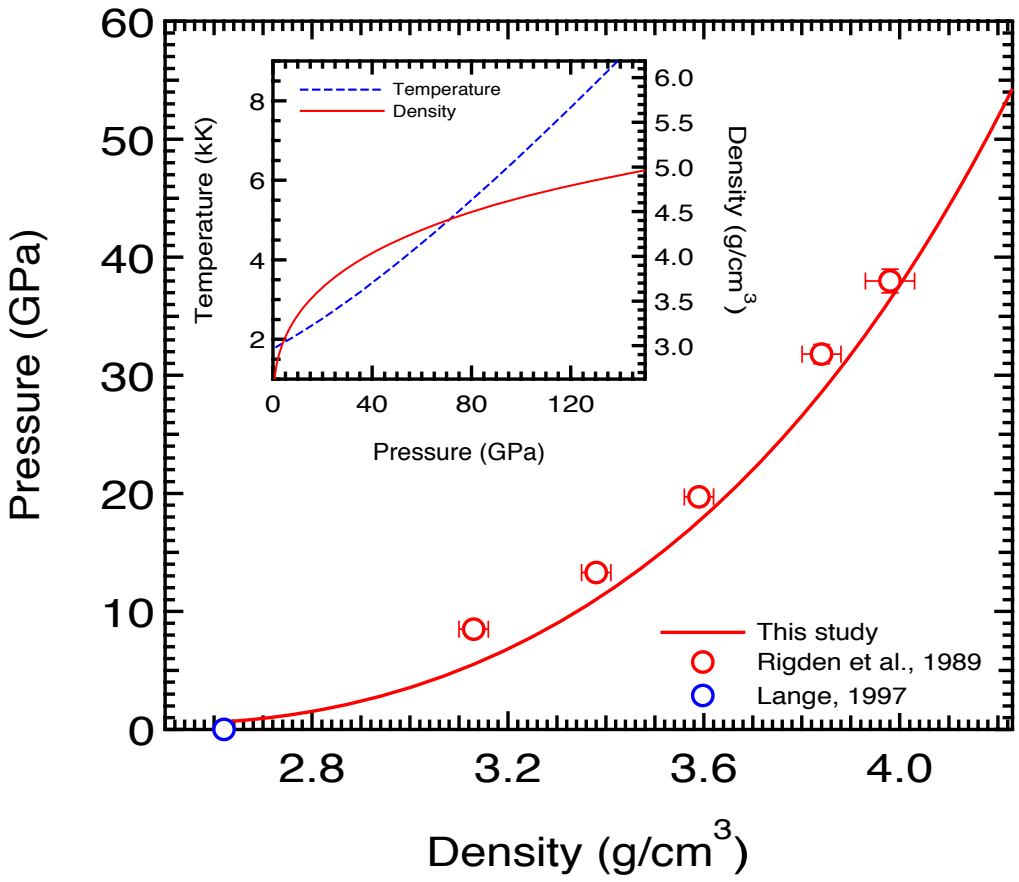

FIGURE 2.7 Comparison of diopside liquid and crystal densities at 2400 K. The crystal density is calculated from (Stixrude and Lithgow-Bertelloni, 2005). The Si-O coordination number in the liquid (Figure 2.2a) is indicated on the right hand axis. The sudden increases in density along the blue curve are due to solid-solid phase changes: diopside (4) = garnet-majorite (4,6) + $CaSiO_3$ perovskite (6) at 16.8 GPa, and garnet-majorite (4,6) = $CaSiO_3$ perovksite (6) + $MgSiO_3$ perovksite (6) at 22.5 GPa, where the numbers in parentheses indicate the Si-O coordination number.

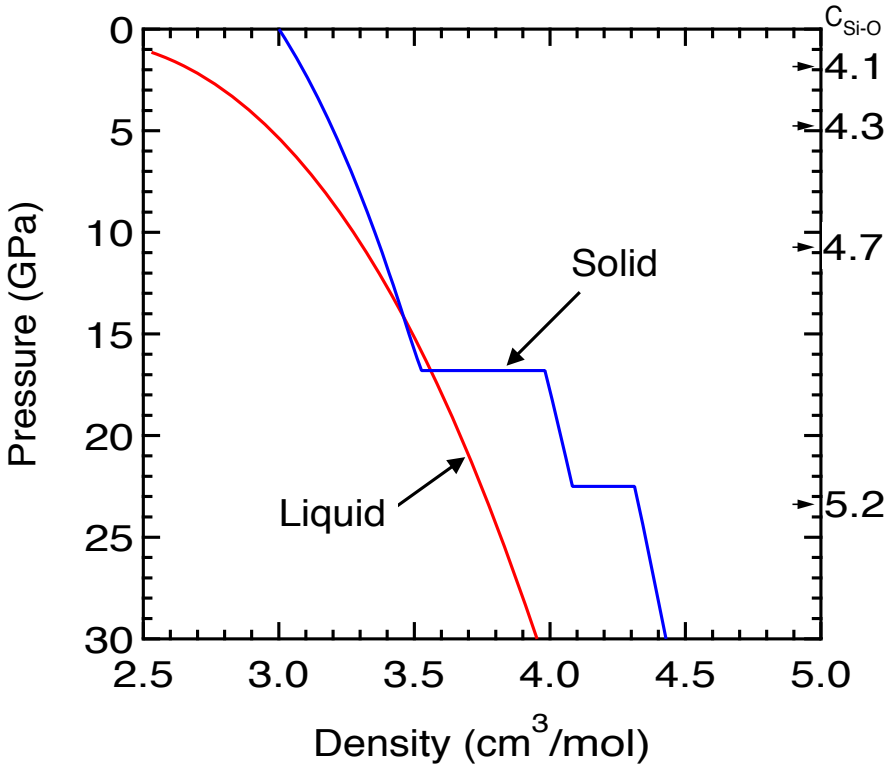

References

Ai, Y. and Lange, R.A., 2007. The compressibility of CaO-MgO-Al_2O_3-SiO_2 liquids from new acoustic velocity measurements: reevaluation of the equation of state of $CaMgSi_2O_6$-$CaAl_2Si_2O_8$ liquids to 25 GPa. Journal of Geophysical Research, 112: B01201.

Alfe, D., Gillan, M.J. and Price, G.D., 2002. Composition and temperature of the Earth's core constrained by combining ab initio calculations and seismic data. Earth and Planetary Science Letters, 195: 91-98.

Benz, W., Slattery, W.L. and Cameron, A.G.W., 1986. The origin of the Moon and the single-impact hypothesis I. Icarus, 66: 515-535.

Birch, F., 1986. Equation of state and thermodynamic parameters of NaCl to 300 kbar in the high-temperature domain. Journal of geophysical research, 91(B5): 4949-4954.

Boehler, R., 2000. High-pressure experiments and the phase diagram of lowermantle and core constituents. Reviews of Geophysics, 38: 221–245.

Canup, R.M. and Asphaug, E., 2001. Origin of the Moon in a giant impact near the end of the Earth's formation. Nature, 412: 708-712.

de Koker, N., Stixrude, L. and Karki, B.B., 2008. Thermodynamics, structure, dynamics, and freezing of Mg_2SiO_4 liquid at high pressure. Geochimica et Cosmochimica Acta, in press.

Fiske, P.S. and Stebbins, J.F., 1994. The structural role of Mg in silicate liquids: A high-temperature ^{25}Mg, ^{23}Na, and ^{29}Si NMR study. American Mineralogist, 79: 848-861.

Francis, G.P. and Payne, M.C., 1990. Finite basis set corrections to total energy pseudopotential calculations. Journal of Physics - Condensed Matter 2: 4395-4404.

Garnero, E.J. and Helmberger, D.V., 1995. On seismic resolution of lateral heterogeneity in the Earth's outermost core. Physics of the Earth and Plantary Interior, 88: 117-130.

Gasparik, T., 1996. Melting experiments on the enstatite-diopside join at 70-224 kbar, including the melting of diopside. Contributions to Mineralogy and Petrology, 124: 139-153.

George, A.M. and Stebbins, J.F., 1998. Structure and dynamics of magnesium in silicate melts: A high-temperature ^{25}Mg NMR study. American Mineralogist, 83: 1022-1029.

Haggerty, S.E. and Sautter, V., 1990. Ultradeep (greater than 300 kilometers), ultramafic upper mantle xenoliths. Science, 248(993-996).

Herzberg, C., 1995. Generation of plume magma through time: an experimental perspective. Chemical Geology, 126: 1-16.

Karki, B.B., Bhattarai, D. and Stixrude, L., 2007. First-principles simulations of liquid silica: Structural and dynamical behavior at high pressure. Physical Review B, 76(10): 104205.

Karki, B.B., Stixrude, L. and Wentzcovitch, R.M., 2001. High-Pressure Elastic Properties of Major Materials of Earth's Mantle from First Principles. Reviews of Geophysics, 39: 507-534.

Kohn, W. and Sham, L.J., 1965. Self-consistent equations including exchange and correlation effects. Physical Review, 140: A1133–A1138.

Kresse, G. and Furthmüller, J., 1996a. Efficiency of ab-initio total energy calculations for metals and semiconductors. Computational Material Science, 6: 15-50.

Kresse, G. and Furthmüller, J., 1996b. Efficient iterative schemes for ab-initio total energy calculations using a plane-wave basis set. Physical Review B, 54: 11,169–11,186.

Kresse, G. and Hafner, J., 1993. Ab initio molecular-dynamics for liquid metals. Physical Review B, 47: 558–561.

Lange, R.A., 1997. A revised model for the density and thermal expansivity of K_2O-Na_2O-CaO-MgO-Al_2O_3-SiO_2 liquids from 700 to 1900 K: extension to crustal magmatic temperatures. Contributions to Mineralogy and Petrology, 130: 1-11.

Lange, R.A. and Carmichael, I.S.E., 1987. Densities of Na_2O-K_2O-MgO-FeO-Fe_2O_3-Al_2O_3-TiO_2-SiO_2 liquids – new measurements and derived partial molar properties. Geochimica et Cosmochimica Acta, 51: 2931-2946.

Lange, R.A. and Navrotsky, A., 1992. Heat capacities of Fe_2O_3-bearing silicate liquids. Contributions to Mineralogy and Petrology, 110: 311-320.

Matsui, M., 1996. Molecular dynamics simulation of structures, bulk moduli, and volume thermal expansivities of silicate liquids in the system CaO-MgO-Al_2O_3-SiO_2. Geophysical Research Letters, 23(4): 395-398.

McQuarrie, D.A., 1976. Statistical Mechanics. Harper and Row, New York.

Miller, G.H., Stolper, E.M. and Ahrens, T.J., 1991. The equation of state of a molten komatiite 2: Application to komatiite petrogenesis and the hadean mantle Journal of Geophysical Research, 96(B7): 11,849-11,864.

Mori, J. and Helmberger, D.V., 1995. Localized boundary layer below the mid-Pacific velocity anomaly identified from a PcP precursor. Journal of Geophysical Research, 100(B10): 20359-20365.

Mosenfelder, J.L., Asimow, P.D. and Ahrens, T.J., 2007. Thermodynamic properties of Mg_2SiO_4 liquid at ultra-high pressures from shock measurements to 200 GPa on forsterite and wadsleyite. Journal of Geophysical Research, 112(B6): B06208.

Nosé, S., 1984. A unified formulation of the constant temperature molecular-dynamics methods. Journal of Chemical Physics, 81(1): 511-519.

Oganov, A.R., Brodholt, J.P. and Price, G.D., 2001. The elastic constants of $MgSiO_3$ perovskite at pressures and temperatures for the Earth's mantle. Nature 411: 934-937.

Revenaugh, J. and Meyer, R., 1997. Seismic evidence of partial melt within a possibly ubiquitous low-velocity layer at the base of the mantle. Science, 277: 670-673.

Rigden, S.M., Ahrens, T.J. and Stolper, E.M., 1989. High pressure equation of state of molten anorthite and diopside. Journal of Geophysical Research, 94: 9508-9522.

Ross, M. and Rogers, F.J., 1985. Structure of dense shock-melted alkali-halides: evidence fro a continuous pressure-induced structural transition in the melt. Physical Review B, 31(3): 1463-1468.

Scarfe, C.M. and Takahashi, E., 1986. Melting of garnet peridotite to 13 GPa and the early history of the upper mantle. Nature, 322: 354-356.

Stebbins, J.F., Carmichael, I.S.E. and Moret, L.K., 1984. Heat Capacities and entropies of silicate liquids and glasses. Contribution to Mineralogy and Petrology, 86: 131-148.

Stebbins, J.F. and McMillan, P., 1989. Five- and six-coordinated Si in $K_2Si_4O_9$ glass quenched from 1.9 GPa and 1200 ^oC. American Mineralogist, 74: 965-968.

Stixrude, L. and Karki, B., 2005. Structure and freezing of $MgSiO_3$ liquid in Earth's lower mantle. Science 310: 297-299.

Stixrude, L. and Lithgow-Bertelloni, C., 2005. Thermodynamics of mantle minerals - I. physical properties. Geophysical Journal International, 162: 610-632.

Stolper, E., Walker, D., Hager, B.H. and Hays, J.F., 1981. Melt segregation from partially molten source regions: The importance of melt density and source region size. Journal of Geophysical Research, 80(B7): 6261-6271.

Tallon, J.L., 1979. Pressure-dependence of melting temperatures for alkali-halides. Physics Letters A, 72: 150-152.

Waseda, Y. and J.M.Toguri, 1977. The structure of molten binary silicate systems CaO-SiO_2 and MgO-SiO_2. Metallurgical Transactions B - Process Metallurgy, 8B: 563-568.

Xue, X., Stebbins, J.F., Kanzaki, M. and Tronnes, R.G., 1989. Silicon coordination and speciation changes in a silicate liquid at high pressures. Science, 245: 962-964.

CHAPTER III

DYNAMICS OF DIOPSIDE LIQUID AT HIGH PRESSURES

3.1 Abstract

The dynamics of diopside liquid at lower mantle conditions has been investigated using first principles molecular dynamics simulations with density functional theory in the local density approximation and the ultra-soft plane-wave pseudopotential method. The total and self diffusion coefficients exhibit an unusual pressure dependence, first decreasing with increasing pressure, than increasing, and finally decreasing again at the highest pressures. This pattern is explained by the pressure-induced decrease in the number of excess non-bridging oxygens at low pressure, and the increase in the number of 5-fold coordinated silicons at higher pressures. Mg has a slightly higher self-diffusion coefficient than Ca, both of which are slightly more diffusive than O, and Si. The average activation energy over the temperature range 3000-6000 K is lower than that found experimentally at lower temperatures, consistent with non-Arrhenian behavior.

3.2 Introduction

Silicate liquids are primary agents of terrestrial chemical differentiation and play an essential role in geological processes, such as mantle metasomatism and magma generation. Evidence from deep-seated xenoliths (Haggerty and Sautter, 1990), and seismological observations of low velocity zones at the base of the upper mantle (Revenaugh and Sipkin, 1994) and at the core-mantle boundary (Williams and Garnero, 1996), suggest that silicate liquids may exist over a much wider pressure range than the present-day magma genetic zone. Liquids may have been even more widespread in the past, when the Earth was presumably hotter; the moon-forming impact may have melted the Earth completely (Canup and Asphaug, 2001).

Among the important properties of silicate liquids that remain unknown over most of the mantle pressure regime are their dynamic properties. We address the chemical diffusivity here, which governs the rate of chemical reaction of melts with their surroundings. In many cases the time-scale for equilibration may be comparable to the time-scale of melt transport, producing melt compositions that depend not only on the composition of the source region, but also the rate of porous flow (Spiegelman and Kelemen, 2003). The diffusivity is also related to the viscosity, which governs the mobility of the melt. Many studies have shown that diffusivity and viscosity are inversely related to each other (Reid et al., 2003; Shimizu and Kushiro, 1984). In many cases, the relationship is accurately quantified by the Eyring relation (Eyring, 1936)

$$\eta = \frac{kT}{D\lambda} \tag{1}$$

where η is the viscosity, D is the diffusivity, k is the Boltzmann constant, and T is temperature, and λ is the jump distance.

The influence of pressure on chemical diffusion and viscosity in silicate liquids is remarkably rich. Experiments (Kushiro, 1976) and subsequently molecular dynamics simulations (Angell et al., 1982) showed that in some compositions, the diffusivity increases and the viscosity decreases on increasing pressure. This behavior confounds intuition based on simple ionic liquids (e.g. alkali halides) that increasing pressure should decrease bond lengths and shrink diffusion pathways, thereby decreasing the rate of diffusion. The anomalous pressure dependence is most pronounced in highly polymerized and Al-rich compositions, and absent in some depolymerized compositions (Poe et al., 1997). High pressure measurements show that at sufficiently high pressure, the trend reverses and the diffusivity does begin to decrease with increasing pressure, producing a pressure at which the diffusivity is a maximum (Poe et al., 1997). Much attention has been focused on the origin of this diffusivity maximum, particularly in highly polymerized melts. But these compositions are probably not representative of melts present at depths greater than the present-day magma genetic zone. Deeper melts are likely less polymerized, and much less is known about their dynamics at high pressure.

A remarkable finding in one relatively de-polymerized composition, diopside, shows precisely the opposite behavior: chemical diffusion initially decreases with pressure, reaches a minimum value and then increases (Reid et al., 2001). At still higher pressure, the diffusivity presumably begins to decrease again, but this regime lies beyond that of the experiments. A recent study of a peridotitic liquid showed the same pattern:

viscosity initially increasing with increasing pressure, reaching a maximum and then decreasing (Liebske et al., 2005). The origin of this behavior is unclear.

In this study, the self-diffusion coefficients of diopside liquid were investigated across the entire mantle pressure-temperature regime by first principles molecular dynamics (FPMD) simulations, which have been successfully used to study structure, equation of state, and thermodynamics properties of silicate liquid (Stixrude and Karki, 2005; Sun et al., 2008a). Possible reasons for anomalous variations of the diffusivity with pressure are found in pressure-induced changes in the liquid structure.

3.3 Computational methods

First principles molecular dynamics simulations were performed to calculate the diffusivity of diopside liquid using Vienna ab initio simulation package (VASP) (Kresse and Furthmüller, 1996a; Kresse and Furthmüller, 1996b; Kresse and Hafner, 1993). The calculations are based on density functional theory (Kohn and Sham, 1965) in the local density approximation (LDA) and the ultra-soft plane-wave pseudopotential method.

Self-diffusion coefficiens are computed from the same first principles molecular dynamics simulations of our earlier study of the struture and equation of state (Sun et al., 2008a)

The self-diffusion coefficient of atom type α, D_α, is computed via the Einstein relation

$$6D_\alpha t = \lim_{t\to\infty}\left\langle \left(\vec{r}_\alpha(t+t_0) - \vec{r}_\alpha(t_0)\right)^2 \right\rangle, \quad (2)$$

where r is position, and the right-hand side represents the mean-squared displacement over the time interval t measured from the origin time t_0. The angle brackets denote an average over all atoms of type α and over origin time t_0. The total self-diffusion coefficient, D is obtained by including atoms of all types in the summation. The relationship is valid in the limit of long time intervals. At short time intervals, the motion of the atoms is ballistic, rather than diffusive and the mean-squared displacement goes like t^2 (Allen and Tildesley, 1987). The coefficient D_α is determined by fitting a straight line to the linear portion of the mean-squared displacement vs. time relationship, excluding the initial ballistic portion.

To further examine the possible influence of finite system size on our computed self-diffusion coefficients, we compute values in the limit of infinite system size according to the hydrodynamic scaling (Yeh and Hummer, 2004)

$$D_L = D_\infty - \frac{k_B T \xi}{6\pi\eta L} \tag{3}$$

where D_L is the calculated diffusion coefficient in a periodic system with translational repeat distance L, D_∞ is infinite diffusion coefficient, k_B is the Boltzmann constant, T is temperature, ξ=2.837297, and η is the shear viscosity. This scaling, which predicts that the self-diffusion coefficient should increase with increasing system size as $N^{1/3}$ agrees well with simulation studies in other systems (de Koker et al., 2008; Zhang et al., 2004). If we combine Eq. (3) with an estimate of the viscosity based on the Eyring relation (Eq. 1) we find

$$D_L = D_\infty\left(1 - \frac{\xi\lambda}{6\pi L}\right) \tag{4}$$

We use a value of the jump distance λ = 4.5 Å determined from measurements of diffusion and viscosity on diopside liquid (Reid et al., 2003).

3.4 Results

The results of diffusion coefficients of $CaMgSi_2O_6$ liquid are showed in Table 3.1. The temporal evolution of the mean-squared displacement, and the derived self-diffusion coefficients are shown in Figures 3.1 - 3.6. At 3000 K, the individual and total self-diffusion coefficients all show the same pattern with increasing pressure: the value of *D* initially decreases with pressure, then increases and finally decreases again. At higher temperatures, these trends are present but less pronounced (Si self-diffusion) or absent, being replaced by a monotonic decrease with increasing pressure. Even at 3000 K, the non-monotonic variations in *D* with pressure are subtle and, except for the overall tendency for *D* to decrease with increasing pressure, lie within the uncertainties of our results.

Despite the non-monotonic variations noted above, we have found that our results can be fit to within error by the Arrhenius relation (Figure 3.2 – 3.6),

$$D(P,T) = D_0 \exp\left(-\frac{E^* + PV^*}{RT}\right) \quad (5)$$

where D_0 is pre-exponential constant, E^* is the activation energy, and V^* is the activation volume. The results of D_0, E^*, V^* are showed in Table 3.2. This manner of describing our results is useful for comparison to experimental values of activation energy and volume.

We find that system size has relatively little effect on the values of the self-diffusion coefficient, and less than the uncertainty in our results. For example, at low pressure and 3000 K, the difference between our 80 atom results and the infinite system result is found to be 7 % by Eq. 4, consistent with our findings in simulations with twice the number of atoms (160).

3.5 Discussions

Our simulations reveal the origin for the unusual pressure dependence of the diffusion coefficient in less polymerized liquids. Two features must be explained: 1) the local maximum in *D* that occurs near 9 GPa and 2) the local minimum in *D* that occurs near 5 GPa. We attribute the local maximum in the diffusivity at 9 GPa to the presence of five-fold coordinated silicons. These represent transition states that facilitate diffusion because of their low activation energy barriers to Si-O bond breaking and reformation. Indeed, we find that the fraction of five-fold coordinated silicons increases with increasing pressure up to ~14 GPa, similar to the highest pressure measured in the experiments of Reid et al. (2001), at which *D* is found still to be increasing with pressure, and somewhat higher than the pressure of the local maximum in *D* in our simulations. Thus we find that the pressure-induced increase in the abundance of five-fold coordinated silicons are important for understanding the pressure dependence of *D* in polymerized and less polymerized melts.

The local minimum in *D* appears to be unique to less polymerized liquids, such as diopside and peridotite. We attribute this feature to a pressure-induced change in the

coordination environment of the network modifiers. At low pressure, MgO_5 groups are most abundant. We envision these playing a similar role to SiO_5 groups: as transition states that facilitate diffusion. With increasing pressure, 5-fold coordinated Mg decrease rapidly in abundance, and this rapid decrease accounts for the initial decrease in the diffusivity.

The activation energy that we find in diopside melt is considerably lower than that found in previous experimental studies (Reid et al., 2001; Shimizu and Kushiro, 1984; Tinker et al., 2003). We attribute this to non-Arrhenian temperature dependence of the diffusivity. Although our results can be described by the Arrhenius relation to within uncertainty, we cannot rule out a temperature dependent activation energy. In fact experimental data on the viscosity of diopside liquid show distinctly non-Arrhenian behavior, with an activation enthalpy that decreases with increasing temperature (Taniguchi, 1995), consistent with the lower value of the activation enthalpy that we find in our simulations.

The slightly greater self-diffusion coefficient of Mg as compared with Ca is consistent with previous experimental results. Nakamura and Kushiro, 1998 (Nakamura and Kushiro, 1998) found that the self-diffusion coefficient increases systematically with decreasing ionic radius for ions of the same charge for a large number of ions including Mg, Ca, and rare earth elements. They found that the self-diffusion coefficient of Mg was 20 % greater than that of Ca, quantitatively consistent with our findings. On the other hand, the only previous molecular dynamics study of diffusion in diopside melt obtained very different results (Angell et al., 1987). These authors found the self-diffusion coefficient of Ca to be a factor of two greater than that of Mg, and that of Si to

be 50 % less. They also did not find the local minimum in the diffusivity that we find. As this study was based on semi-empirical pair potentials, the differences with our study emphasize the importance of the first principles molecular dynamics approach for obtaining reliable results.

3.6 Conclusions

We have investigated the dynamics of diopside liquid at lower mantle conditions by first principles molecular dynamics simulations. The results reproduce the unusual pressure dependence of the diffusivity in diopside liquid seen experimentally, extend these to much higher pressures, and provide an explanation in terms of pressure-induced changes in liquid structure. The activation energy is lower than that found in previous experimental studies, consistent with expected non-Ahrrenian behavior and the difference in the temperature range between the experiments and our calculations. Our results support the pattern of increasing diffusivity with decreasing ionic radius found in previous studies.

3.7 Acknowledgements

This research was supported by the National Science Foundation under grants EAR-0409074 and EAR-0409121. Computing facilities were provided by CCT at Louisiana State University.

TABLE 3.1 Results of diffusion coefficients of $CaMgSi_2O_6$ liquid. Simulations at 3000 K and the highest pressure (*) produced a glass with no significant diffusion within our resolution.

T (K)	P (GPa)	Total (m^2/s)	Si-self (m^2/s)	O-self (m^2/s)	Ca-self (m^2/s)	Mg-self (m^2/s)
3000	3.28 ± 1.43	3.09e-09 ± 9.95e-10	1.98e-09 ± 4.57e-10	3.23e-09 ± 4.57e-10	3.52e-09 ± 4.57e-10	3.99e-09 ± 4.57e-10
3000	4.94 ± 1.43	2.07e-09 ± 6.99e-10	1.07e-09 ± 5.53e-10	2.01e-09 ± 9.48e-10	2.65e-09 ± 1.41e-09	3.89e-09 ± 1.74e-09
3000	9.00 ± 1.46	3.03e-09 ±1.43e-09	2.04e-09 ± 1.73e-09	3.35e-09 ± 1.46e-09	1.63e-09 ± 1.55e-09	4.56e-09 ± 1.31e-09
3000	17.53 ± 1.45	1.85e-09 ± 1.02e-09	1.5e-09 ± 6.39e-10	1.84e-09 ± 9.4e-10	2.2e-09 ± 1.85e-09	2.24e-09 ± 3.69e-09
3000	34.49 ± 1.54	7.73e-10 ± 8.42e-10	6.52e-10 ± 5.39e-10	8.75e-10 ± 9.59e-10	7.59e-10 ± 1.06e-09	4.18e-10 ± 1.01e-09
3000	70.04 ± 1.61	2.94e-10 ± 7.79e-10	1.2e-10 ± 7e-10	4.01e-10 ± 7.24e-10	8.44e-11 ± 5.94e-10	2.11e-10 ± 1.48e-09
3000*	158.74 ± 1.44	3.14e-11 ± 3.81e-10	2.48e-11 ± 2.45e-10	3.37e-11 ± 4.35e-10	2.58e-11 ± 3.39e-10	3.58e-11 ± 4.81e-10
4000	4.73 ± 1.43	1.17e-08 ± 2.35e-09	9.86e-09 ± 1.65e-10	1.2e-08 ± 1.65e-09	1.27e-08 ± 1.65e-09	1.3e-08 ± 1.65e-09
4000	7.10 ± 1.43	8.97e-09 ± 1.37e-09	7.19e-09 ± 1.52e-09	8.83e-09 ± 2.27e-09	1.05e-08 ± 5.22e-09	1.19e-08 ± 3.03e-09
4000	12.19 ± 1.45	8.22e-09 ± 2.84e-09	4.32e-09 ± 2.46e-09	8.82e-09 ± 3.38e-09	1.17e-08 ± 1.61e-09	8.89e-09 ± 5.98e-09
4000	21.95 ± 1.45	5.31e-09 ± 4.49e-10	4.5e-09 ± 5.32e-10	5.55e-09 ± 7.59e-10	5.21e-09 ± 1.81e-09	5.58e-09 ± 2.87e-09
4000	40.58 ± 1.45	4.02e-09 ± 7.92e-10	4.28e-09 ± 1e-09	4.41e-09 ± 8.63e-10	2.02e-09 ± 1.42e-09	3.16e-09 ± 2.82e-09
4000	77.02 ± 1.42	4.37e-10 ± 8.46e-10	2.7e-10 ± 6.55e-10	5.28e-10 ± 9.98e-10	3.84e-10 ± 7.95e-10	2.8e-10 ± 1.11e-09
4000	160.08 ± 1.54	1.73e-10 ± 3.48e-10	8.81e-11 ± 2.4e-10	1.82e-10 ± 3.24e-10	2.82e-10 ± 7.16e-10	1.76e-10 ± 7.67e-10
6000	9.76 ± 1.43	3.64e-08 ± 2.35e-09	3.26e-08 ± 1.15e-09	3.97e-08 ± 1.15e-09	2.63e-08 ± 1.15e-09	3.43e-08 ± 1.15e-09
6000	12.42 ± 1.44	3.23e-08 ± 3.75e-09	2.29e-08 ± 3.28e-09	3.65e-08 ± 5.63e-09	1.85e-08 ± 2.66e-09	3.94e-08 ± 5.96e-09
6000	19.06 ± 1.42	2.42e-08 ± 6.89e-09	1.26e-08 ± 5.43e-09	2.81e-08 ± 8.12e-09	2.52e-08 ± 5.5e-09	2.36e-08 ± 6.87e-09
6000	31.05 ± 1.44	2.04e-08 ± 1.39e-09	1.67e-08 ± 3.65e-09	2.19e-08 ± 1.44e-09	1.77e-08 ± 2.74e-09	2.12e-08 ± 6.56e-09
6000	52.78 ± 1.43	1.49e-08 ± 1.94e-09	1.35e-08 ± 2.56e-09	1.7e-08 ± 2.48e-09	1.13e-08 ± 4.08e-09	8.99e-08 ± 4.91e-09
6000	93.98 ± 1.50	6.81e-08 ± 2.09e-09	5.13e-09 ± 2.02e-09	7.7e-09 ± 2.4e-09	6.37e-09 ± 4.14e-09	5.26e-08 ± 2.7e-09
6000	180.12 ± 2.46	3.29e-08 ± 3.85e-10	2.45e-09 ± 6.75e-10	3.74e-09 ± 5.75e-10	2.96e-09 ± 6.08e-10	2.62e-08 ± 1.72e-09

TABLE 3.2 Fitting parameters in Arrhenius relation. The parameters are calculated from all the results. [1]1783 ~ 2037 K (Tinker et al., 2003), [2] 2273 K(Reid et al., 2001).

	D_0 (10^{-9} m^2/s)	E^* (kJ/mol)	V^* (cm^3/mol)
Total	475 ± 87	127.73 ± 6.63	0.75 ± 0.05
Si-self	494 ± 128	130.29 ± 9.05	0.88 ± 0.08
O-self	563 ± 92	129.46 ± 6.07	0.77 ± 0.05
Ca-self	245 ± 60	104.51 ± 8.75	0.75 ± 0.07
Mg-self	245 ± 64	108.01 ± 6.39	0.95 ± 0.08
Si-self [1]	0.0036 ± 0.0004	227 ± 13	-2.3 ± 0.4
O-self [1]	0.0042 ± 0.0004	215 ± 13	-2.1 ± 0.4
O-self [2]	0.39 ~ 0.98	267	-

FIGURE 3.1 Mean square displacement of all atoms in $CaMgSi_2O_6$ liquid at (a) 3000 K, (b) 4000 K, and (c) 6000 K.

(a)

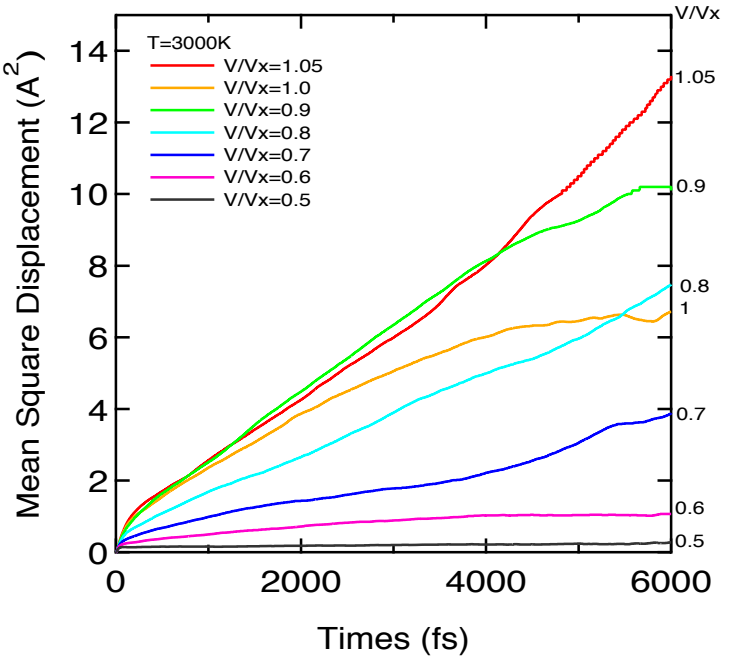

(b)

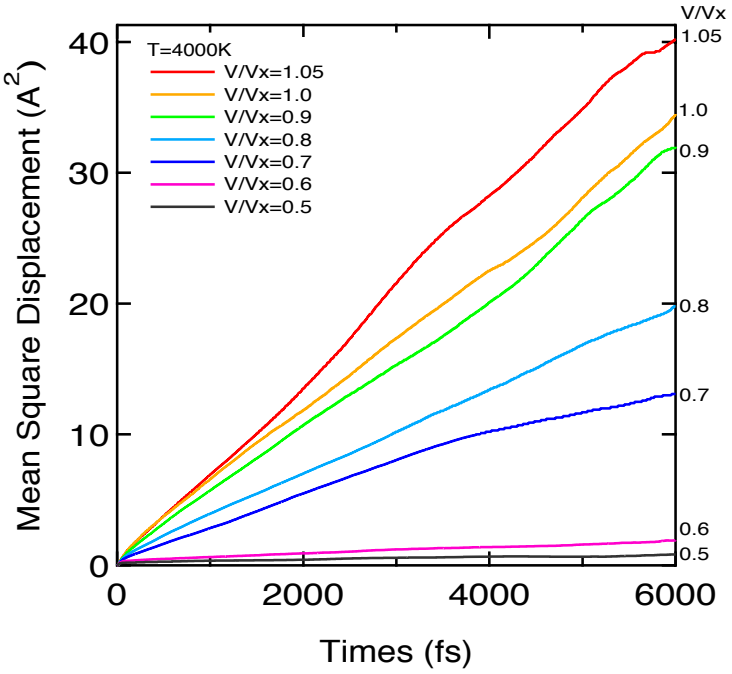

FIGURE 3.1 (continued)

(c)

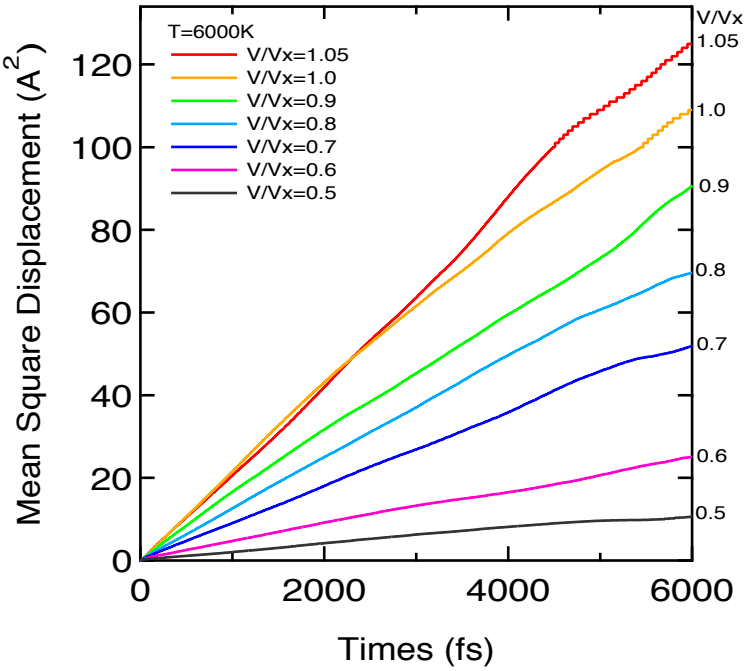

FIGURE 3.2 The pressure dependence of total diffusion coefficient in $CaMgSi_2O_6$ liquid at 3000 K (in blue), 4000 K (in green), and 6000 K (in red). The lines are fit via Arrhenius relation.

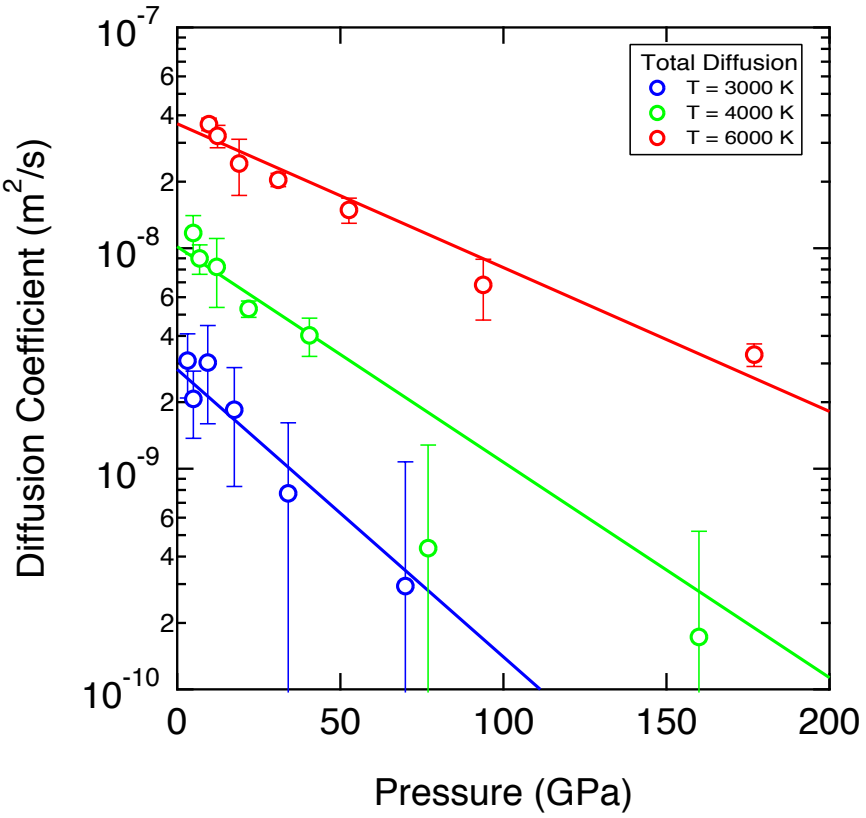

FIGURE 3.3 The pressure dependence of silicon self-diffusion coefficient in $CaMgSi_2O_6$ liquid at 3000 K (in blue), 4000 K (in green), and 6000 K (in red). The solid lines fit all results via Arrhenius relation. The dashed lines fit the results at lowest pressure results.

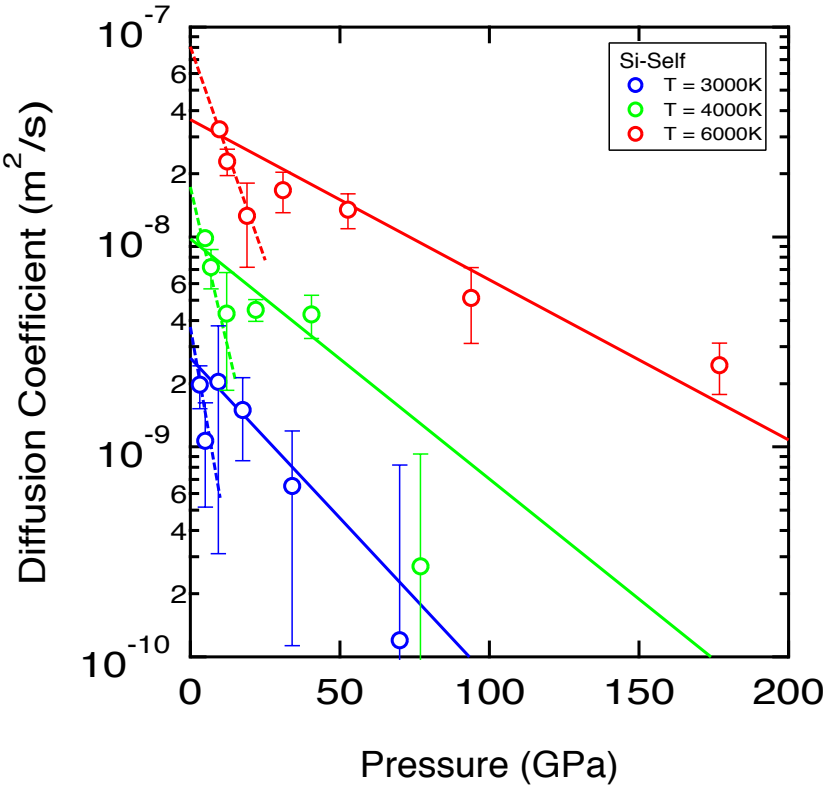

FIGURE 3.4 The pressure dependence of oxygen self-diffusion coefficient in $CaMgSi_2O_6$ liquid at 3000 K (in blue), 4000 K (in green), and 6000 K (in red). Lines are from the fitted Arrhenius relation. (b) Detail of low pressure behavior including comparison with experimental results (solid points) (Reid et al., 2001) corrected by Reid et al. to constant temperature using an activation energy of 267 kJ/mol. (c) Proportion of five-fold coordination Mg (dashed) and five-fold coordinated Si (solid) at 3000 K (blue), 4000 K (green) and 6000 K (red).

(a)

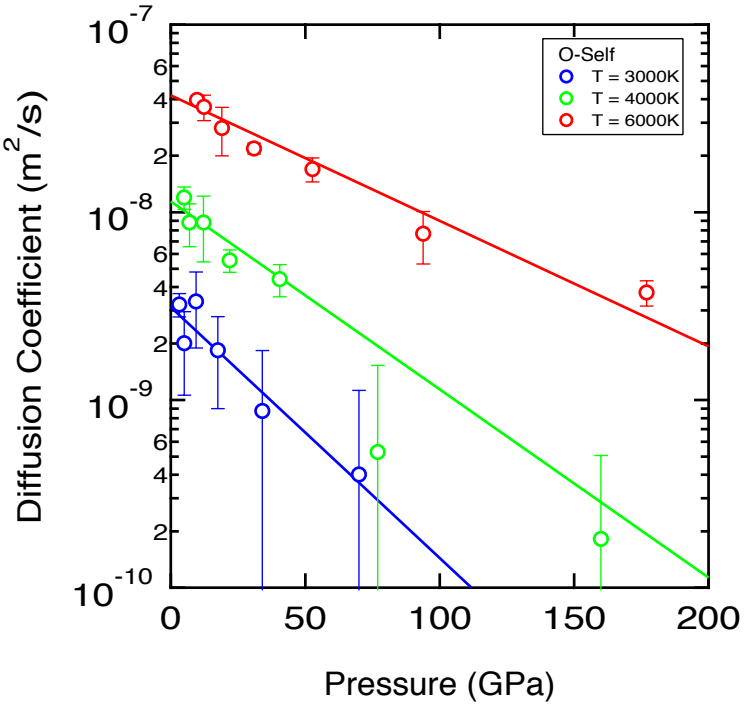

FIGURE 3.4 (continued)

(b)

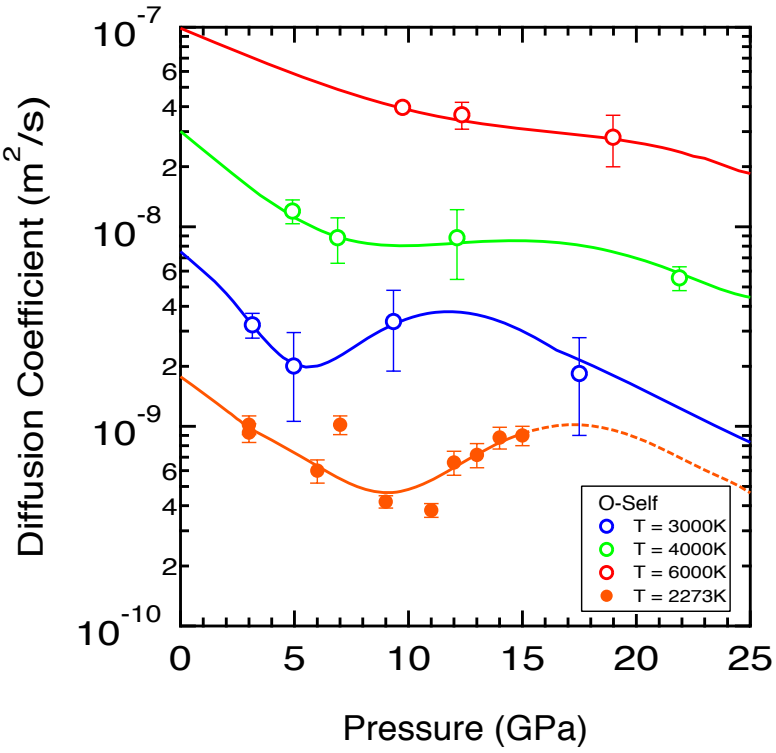

(c)

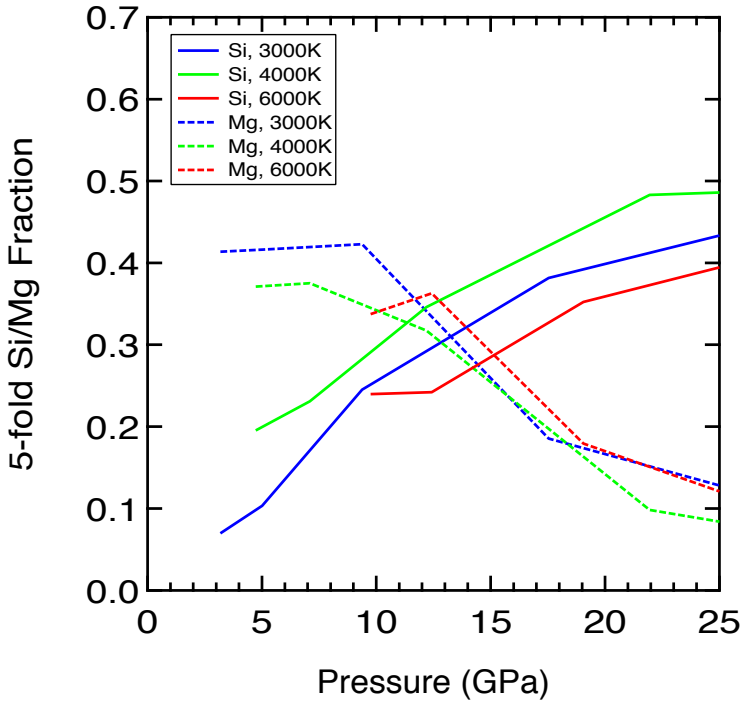

FIGURE 3.5 The pressure dependence of calcium self-diffusion coefficient in $CaMgSi_2O_6$ liquid at 3000 K (in blue), 4000 K (in green), and 6000 K (in red). Lines are from the fitted Arrhenius relation.

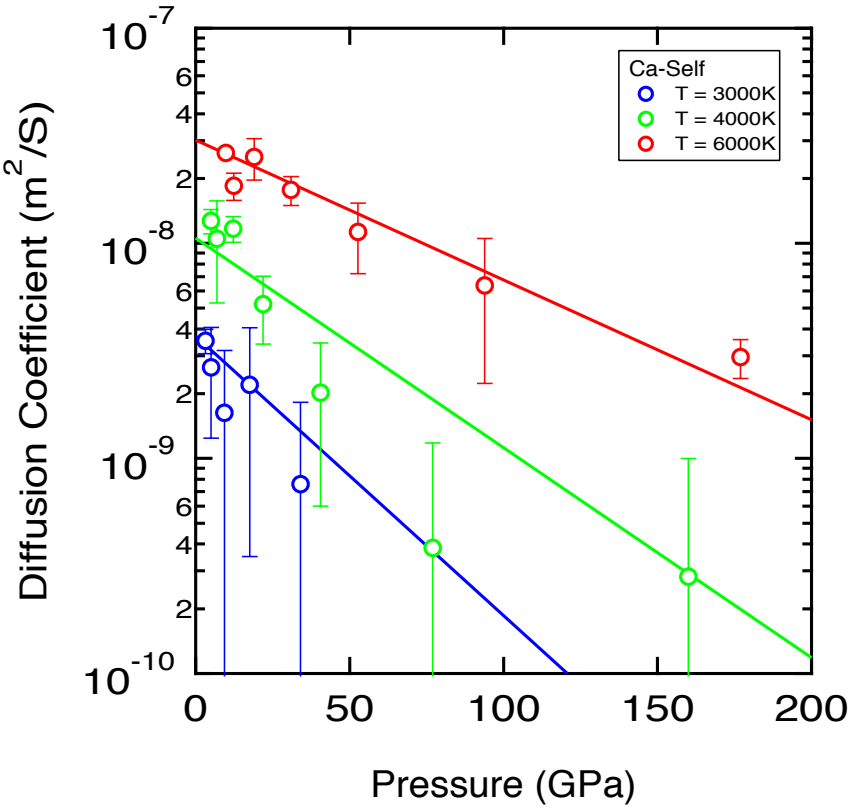

FIGURE 3.6 The pressure dependence of magnesium self-diffusion coefficient in $CaMgSi_2O_6$ liquid at 3000 K (in blue), 4000 K (in green), and 6000 K (in red). Lines are from the fitted Arrhenius relation.

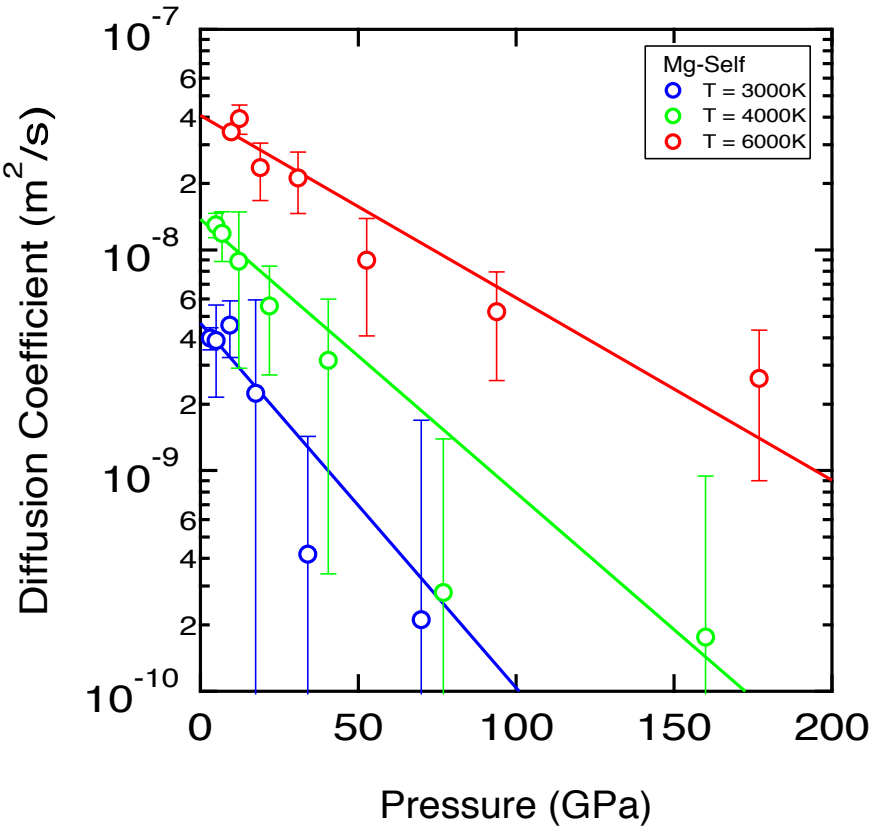

References

Allen, M.P. and Tildesley, D.J., 1987. Computer Simulation of Liquids. Oxford University Press, Oxford.

Angell, C.A., Cheeseman, P.A. and Kadiyala, R.R., 1987. Diffusivity and thermodynamic properties of diopside and jadeite melts by computer simulation studies. Chemical Geology, 62: 83-92.

Angell, C.A., Cheeseman, P.A. and Tamaddon, S., 1982. Pressure enhancement of ion mobilities in liquid silicates from computer simulation studies to 800 kilobars. Science, 218: 885-887.

Canup, R.M. and Asphaug, E., 2001. Origin of the Moon in a giant impact near the end of the Earth's formation. Nature, 412(6848): 708-712.

de Koker, N., Stixrude, L. and Karki, B.B., 2008. Thermodynamics, structure, dynamics, and freezing of Mg_2SiO_4 liquid at high pressure. Geochimica et Cosmochimica Acta, in press.

Eyring, H., 1936. Viscosity, plasticity, and diffusion as examples of absolute reaction rates. Journal of Chemical Physics, 4(4): 283-291.

Haggerty, S.E. and Sautter, V., 1990. Ultradeep (greater than 300 kilometers), ultramafic upper mantle xenoliths. Science, 248: 993-996.

Kohn, W. and Sham, L.J., 1965. Self-consistent equations including exchange and correlation effects. Physical Review, 140: A1133–A1138.

Kresse, G. and Furthmüller, J., 1996a. Efficiency of ab-initio total energy calculations for metals and semiconductors. Computational Material Science, 6: 15-50.

Kresse, G. and Furthmüller, J., 1996b. Efficient iterative schemes for ab-initio total energy calculations using a plane-wave basis set. Physical Review B, 54: 11,169–11,186.

Kresse, G. and Hafner, J., 1993. Ab initio molecular-dynamics for liquid metals. Physical Review B, 47: 558–561.

Kushiro, I., 1976. Changes in viscosity and structure of melt of $NaAlSi_2O_6$ composition at high-pressures. Journal of Geophysical Research, 81(35): 6347-6350.

Lange, R.A. and Carmichael, I.S.E., 1987. Densities of Na_2O-K_2O-MgO-FeO-Fe_2O_3-Al_2O_3-TiO_2-SiO_2 liquids – new measurements and derived partial molar properties. Geochimica et Cosmochimica Acta, 51: 2931-2946.

Liebske, C. et al., 2005. Viscosity of peridotite liquid up to 13 GPa: Implications for magma ocean viscosities. Earth and Planetary Science Letters, 240(3-4): 589-604.

Nakamura, E. and Kushiro, I., 1998. Trace element diffusion in jadeite and diopside melts at high pressures and its geochemical implication. Geochimica et Cosmochimica Acta, 62(18): 3151-3160.

Poe, B.T. et al., 1997. Silicon and oxygen self-diffusivities in silicate liquids measured to 15 gigapascals and 2800 kelvin. Science, 276: 1245-1248.

Reid, J.E., Poe, B.T., Rubie, D.C., Zotov, N. and Wiedenbeck, M., 2001. The self-diffusion of silicon and oxygen in diopside ($CaMgSi_2O_6$) liquid up to 15 GPa. Chemical Geology, 174: 77-86.

Reid, J.E. et al., 2003. The viscosity of $CaMgSi_2O_6$ liquid at pressures up to 13 GPa Physics of the Earth and Planetary interiors, 139: 45-54.

Revenaugh, J. and Sipkin, S.A., 1994. Seismic evidence for silicate melt atop the 410 km mantle discontinuity. Nature, 369(6480): 474-476.

Shimizu, N. and Kushiro, I., 1984. Diffusivity of oxygen in jadeite and diopside melts at high pressures. Geochimica et Cosmochimica Acta, 48: 1295-1303.

Spiegelman, M. and Kelemen, P.B., 2003. Extreme chemical variability as a consequence of channelized melt transport. Geochemistry Geophysics Geosystems, 4: 1055.

Stixrude, L. and Karki, B., 2005. Structure and freezing of $MgSiO_3$ liquid in Earth's lower mantle. Science 310: 297-299.

Sun, N., Stixrude, L. and Karki, B.B., 2008a. High pressure structure and equation of state of diopside liquid. Earth and Planetary Science Letters, to be submitted.

Taniguchi, H., 1995. Universal viscosity equation for silicate melts over wide temperature and pressure ranges. Journal of Volcanology and Geothermal Research, 66(1-4): 1-8.

Tinker, D., Lesher, C.E. and Hutcheon, I.D., 2003. Self-diffusion of Si and O in diopside-anorthite melt at high pressure. Geochemistry Geophysics Geosystems, 67(1): 133-143.

Williams, Q. and Garnero, E.J., 1996. Seismic evidence for partial melt at the base of Earth's mantle. Science, 273(5281): 1528-1530.

Yeh, I.-C. and Hummer, G., 2004. System-size dependence of diffusion coefficients and viscosities from molecular dynamics simulations with periodic boundary conditions. Journal of Physical Chemistry B, 108: 15873-15879.

Zhang, Y., Guo, G., Refson, K. and Zhao, Y., 2004. Finite-size effect at both high and low temperatures in molecular dynamics calculations of the self-diffusion coefficient and viscosity of liquid silica. Journal of Physics: Condensed Matters, 16: 9127-9135.

CHAPTER IV

THERMODYNAMICS OF $CaSiO_3$ LIQUID AND MIXING ON $MgSiO_3$ - $CaSiO_3$ JOIN

4.1 Abstract

The thermodynamics of $CaSiO_3$ liquid have been investigated by first principles molecular dynamics simulations with density functional theory in the local density approximation and ultra-soft plane-wave pseudopotential method. Liquid structure becomes more densely packed on compression: the average Si-O and Ca-O coordination number increase nearly linearly and do not depend significantly on temperature along isochores. The fraction of 3-fold and 4-fold coordinated Si atoms decreases and the fraction of 6-fold, and 7-fold coordinated Si atoms increases on compression. The fraction of 5-fold coordinated Si atoms initially increases on compression and then decreases at the smallest volumes. The pressure is well fitted by Mie-Grüneisen equation of state, with V_0=1.29V_x K_0=12.36 GPa, and K_0'=5.94 at 3000 K. The Grüneisen parameter increases linearly on compression, behavior opposite to mantle crystalline phases, while the heat capacity decreases on compression. We combine our results with

previous results on $MgSiO_3$ and $CaMgSi_2O_6$ compositions to determine the volume of mixing on the $MgSiO_3$-$CaSiO_3$ join. We find that the volume of mixing is zero within uncertainty.

4.2 Introduction

The high-pressure phase of $CaSiO_3$, Ca-perovskite, is thought to be a major lower mantle phase, and has been investigated by many experimental studies (Shim et al., 2000; Shim et al., 2002) and computational simulations (Adams and Oganov, 2006; Caracas and Wentzcovitch, 2005; Jung and Oganov, 2005; Li et al., 2006a; Li et al., 2006b; Stixrude et al., 1996; Stixrude et al., 2007; Zhang et al., 2006). $CaSiO_3$ perovskite is a major component of basalt, a portion of subducting slabs that may be the first to melt on descent into the deep lower mantle. However, the physical properties of $CaSiO_3$ liquid at high pressure are still unknown. Indeed, partial melting may explain the presence of ultra-low velocity zones (ULVZ) at the base of the mantle (Williams and Garnero, 1996), emphasizing the need for exploring the physical properties of melts over the entire mantle pressure regime.

The $MgSiO_3$-$CaSiO_3$ join represents the ideal system for an exploration of the still unknown thermodynamics of mixing of silicate melts at high pressure. This system accounts for more 80 % of the bulk silicate Earth and includes diopside, a major component of model basalt compositions. The system is homovalent, and its subsolidus mixing properties are well characterized.

In this study, we investigated $CaSiO_3$ liquid across the entire mantle pressure-temperature regime by first principles molecular dynamics (FPMD) simulations, which have been successfully used to study enstatite ($MgSiO_3$) liquid (Stixrude and Karki, 2005), and diopside ($CaMgSi_2O_6$) liquid (Sun et al., 2008a; Sun et al., 2008b), among other compositions. We predict the structure and the equation of state of $CaSiO_3$ liquid at high pressure and compare our results with existing lower pressure and lower temperature experiments (Ai and Lange, 2007; Funamori et al., 2004; Lange, 1997; Lange and Carmichael, 1987; Lange and Navrotsky, 1992; Stebbins et al., 1984). To understand the mixing of $MgSiO_3$-$CaSiO_3$ join, the volume of solution is computed by combining my results with previous results on $MgSiO_3$ composition (Stixrude and Karki, 2005).

4.3 Computational Methods

Our simulations of $CaSiO_3$ liquid are based on density functional theory (DFT) (Kohn and Sham, 1965) in the local density approximation (LDA) and the ultra-soft plane-wave pseudopotential method. The computations were performed with the Vienna ab initio simulation package (VASP) (Kresse and Furthmüller, 1996a; Kresse and Furthmüller, 1996b; Kresse and Hafner, 1993). Simulations are performed in the canonical ensemble with a Nosé thermostate (Nose, 1984). The initial condition is an 80-atom pyroxene supercell homogeneously strained to a cubic shape and melted at 6000 K, then isochorically cooled to 4000 K and 3000 K. For the smallest volumes, $V=0.6V_x$ and $V=0.5V_x$, the cell was initially melted at 10,000 K, then isochorically cooled to 6000 K, 4000 K, and 3000 K. For each calculation, the total run duration is 3 picoseconds, with

the last 2.4 picoseconds used to calculated thermodynamic properties. Larger systems (160 atoms) and longer run durations (6 picoseconds) were tested and found to produce results indistinguishable within statistical uncertainty. We explore a range of volumes from the experimental value at the ambient pressure melting point, 86.9 cm3/mol (Lange and Carmichael, 1987) to 38.9 cm3/mol (6 oxygen basis). The volumes are expressed as V/V_X where V_x=77.8 cm^3/mol, the volume of enstatite composition ($Mg_2Si_2O_6$) liquid at the ambient-pressure melting point (Lange and Carmichael, 1987), provides a convenient reference for comparison with our previous results (Stixrude and Karki, 2005; Sun et al., 2008a).

Estimates of the uncertainty (precision) in the internal energy, and pressure take into account the appropriate non-Gaussian statistics via the blocking method (Flyvbjerg and Petersen, 1989). In order to compute solution properties, we must compare at constant pressure, which we do by first fitting simulation results to analytical forms. The resulting uncertainty in the volume at each pressure is estimated as

$$\sigma_V = \frac{\sigma_P}{K_T} V \tag{1}$$

where σ_P is the uncertainty in the pressure from the simulation, K_T is the bulk modulus computed from the fitted equation of state, and V is the volume.

The pressures computed from the FPMD simulations are corrected as in our previous study (Sun et al., 2008a)

$$P(V,T) = P_{MD}(V,T) + P_{Pulay}(V) + P_{emp} \tag{2}$$

where P_{MD} is calculation pressure, P_{Pulay} is Pulay (finite basis set correction), and P_{emp} is an empirical correction. The corrections are calculated with a fully relaxed 20 atom unit cell of wollastonite and a 2x2x2 Monkhorst-Pack k-point mesh. The Pulay pressure

correction varies linearly with volume from 2.53 GPa at $V=V_x$ to 4.56 GPa at $V=V_x/2$, and the empirical correction is found to be 3.73 GPa, using the thermodynamic model of Stixrude and Lithgow-Bertelloni (2005) as an estimate of the static zero-pressure volume.

4.4 Thermodynamics of $CaSiO_3$ liquid

4.4.1 Structure

Si-O and Ca-O coordination numbers (Table 4.1, Figure 4.1-4.3) increase with compression and do not appear to depend systematically on temperature along isochores, which are identical to those found previously for $CaMgSi_2O_6$ liquid (Sun et al., 2008a) and $MgSiO_3$ liquid (Stixrude and Karki, 2005). The liquid shows an average Si-O coordination number of 4.1 at $V=1.12V_x$, which is close to the value found experimentally in silicate glass at ambient pressure (Stebbins and McMillan, 1989; Xue et al., 1989), and an average Si-O coordination number of 6.1 at $V=V_x/2$ (Figure 4.2). The average Ca-O coordination number of $CaSiO_3$ liquid varies from 5.9 at $V=1.12V_X$ to 9.3 at $V=V_X/2$ (Figure 4.3).

We also investigated the Si-O coordination number distribution (Figure 4.4). On compression, the fraction of 3-fold and 4-fold coordinated Si atoms decreases and the fraction of 6-fold, and 7-fold coordinated Si atoms increases. The fraction of 5-fold coordinated Si atoms initially increases on compression and then decreases at the smallest volumes, showing a maximum at $V=0.7V_x$, where the pressure is 47 GPa at 3000 K. At $V/V_x=0.7$, 5-fold coordinated Si are the most abundant. With increasing temperature, the

variety of Si-O coordination environments increases. For example, at $V=V_x$, the proportion of 3-fold and 5-fold coordination increases with increasing temperature.

4.4.2 Equation of State

The equation of state (Table 4.1, Figure 4.5) could be described by the Mie-Grüneisen equation:

$$P(V,T) = P_C(V,T_C) + P_{TH}(V,T) \tag{3}$$

where P_C is reference pressure, T_C is the reference temperature, and $P_{TH}(V,T)$ is the thermal pressure. The equation of state of wollastonite liquid at the reference temperature, 3000 K, is described by the third-order Birch-Murnaghan equation with zero pressure volume $V_0=1.29V_x$, bulk modulus $K_0=12.36$ GPa, and first pressure derivative of the bulk modulus $K_0'=5.94$. The thermal pressure can be described as

$$P_{TH}(V,T) = \frac{\gamma(V)}{V} C_V(V)(T - T_C) \tag{4}$$

where γ is Grüneisen parameter and C_V is isochoric heat capacity.

The Grüneisen parameter is calculated at each volume from the thermodynamic identity

$$\gamma \equiv V\left(\frac{\partial P}{\partial U}\right)_V \tag{5}$$

and C_V is computed at each volume from

$$C_V = \left(\frac{\partial U}{\partial T}\right)_V \tag{6}$$

where U is the internal energy. We find that the relationship between P and U and between U and T is linear along isochores, so that the value of γ and C_V at each volume is

computed from the slope of the best fit line. The Grüneisen parameter γ is 0.47 ± 0.15 at V=1.12V_x as compared with the experimental value: 0.68 ± 0.10, calculated from (Ai and Lange, 2007; Lange, 1997; Lange and Navrotsky, 1992) and increases to 1.08 ± 0.10 at V=V_x/2.

The increase of the Grüneisen parameter with compression is similar to our findings in $CaMgSi_2O_6$ liquid (factor of two over two-fold compression) but smaller than the increase found previously in $MgSiO_3$ liquid over the same range (Stixrude and Karki, 2005) (factor of three). The value of C_V is 4.61 ± 0.01 *Nk* at V=1.12V_x (the experimental value is 4.00 ± 0.10 *Nk* (Lange and Navrotsky, 1992) and 3.60 ± 0.30 *Nk* (Stebbins et al., 1984)), then nearly linearly decreases to 3.24 ± 0.04 *Nk* at V=V_x/2, where N is the number of atom and k is Boltzmann constant.

For comparison with experimental results at ambient conditions, simulation results are shown at the experimental volume, V=86.9 cm^3/mol, of wollastonite liquid at the ambient-pressure melting point, 1817 K (Lange and Carmichael, 1987) (Figure 4.5). We calculated the experimentally observed rate at which pressure increases with temperature along the isochore from experimental values of thermal expansivity (Lange, 1997) and bulk modulus (Ai and Lange, 2007) and the identity

$$\left(\frac{\partial P}{\partial T}\right)_V = \alpha K_T \tag{7}$$

We find agreement between the experimental value computed from Eq. 7 (2.03 ± 0.14 MPa K^{-1}) and the value determined directly from the pressure-temperature relation from our FPMD simulations (2.47 ± 0.21 MPa K^{-1}).

4.5 Mixing on the $MgSiO_3$ - $CaSiO_3$ Join

The volume of solution is

$$\Delta V(P,T) = V_{di}(P,T) - \frac{1}{2}V_{en}(P,T) - \frac{1}{2}V_{wo}(P,T) \quad (8)$$

where the subscripts refer to diopside (di, $CaMgSi_2O_6$), enstatite (en, $Mg_2Si_2O_6$) and wollastonite (wo, $Ca_2Si_2O_6$) compositions. We find that ΔV is identically zero over the entire pressure range of our simulations (maximum magnitude 0.004 cm^3 mol^{-1} Figure 4.8). The uncertainty is ±5 cm^3 mol^{-1} (6 oxygen basis) at zero pressure and decreases with increasing pressure because σ_P varies little with volume and the bulk modulus increases rapidly with increasing pressure.

4.6 Discussion

The most remarkable finding of our study is the ideality of the volume on the $MgSiO_3$-$CaSiO_3$ join. This is in contrast to the sub-solidus system in which the volumes at ambient conditions of crystalline enstatite (66.676 cm^3 mol-1), diopside (66.039 cm^3 mol^{-1}) and wollastonite (79.107 cm^3 mol^{-1}) yield ΔV=-4.85 cm^3 mol^{-1} (Smyth and McCormick, 1995). It is now well established that ideal mixing of simple oxides represents experimental measurements of silicate liquid volumes in this system and many others very well (Lange, 1997; Lange and Carmichael, 1987). However, there has been no basis for testing the assumption of ideality at high pressure in any system except for

the diopside-anorthite system, in which the volume appears to mix ideally at least up to 40 GPa (Rigden et al., 1989).

Our predicted liquid structures help to explain the small volume of mixing. We find that the structures across this join are remarkably similar. When compared at constant volume, cation-oxygen coordination numbers are indistinguishable. There are many other similarities as well. The equation of state of all liquids are well represented by the Mie-Grüneisen equation of state with a Grüneisen parameter increasing on compression.

4.7 Conclusions

First principles molecular dynamics simulations were performed for wollastonite liquid up to lower mantle conditions. We examined the structure and equation of state with density functional theory in the local density approximation and the ultra-soft plane-wave pseudopotential method. The liquid structure is much more densely packed on compression. The average Si-O and Ca-O coordination numbers increase with compression. The Si-O coordination number changes from 4 at lower pressure to 6 at higher pressure and Ca-O coordination number changes from 6 at lower pressure to 10 at higher pressure. The equation of state of wollastonite liquid could be well fitted by Mie-Grüneisen equation with a Grüneisen parameter that increases on compression. The volume of solution on the $MgSiO_3$-$CaSiO_3$ join is zero across the entire pressure range of our investigation, supporting the extension of models based on ideal mixing of simple oxides (Lange and Carmichael, 1987) to the base of the mantle.

4.8 Acknowledgements

This research was supported by the National Science Foundation under grants EAR-0409074 and EAR-0409121. Computing facilities were provided by CCT at Louisiana State University.

TABLE 4.1 Results of first principles molecular dynamics simulations of $CaSiO_3$ liquid.

T(K)	V/Vx	ρ(g/cm^3)	P(GPa)	sP(GPa)	E(eV)	sE(eV)	H(eV)	sH(eV)
3000	1.12	2.67	4.16	1.49	-575.303	1.805	-545.318	10.923
3000	1	2.78	8.59	1.46	-578.682	.576	-523.254	9.444
3000	0.9	3.09	14.19	1.47	-579.620	1.427	-497.251	8.649
3000	0.8	3.48	25.43	1.53	-575.385	.589	-444.151	7.910
3000	0.7	3.98	45.94	1.55	-569.817	1.956	-362.380	7.255
3000	0.6	4.64	87.82	1.44	-538.313	.825	-198.409	5.648
3000	0.5	5.57	183.11	1.45	-465.638	1.006	124.956	4.775
4000	1.12	2.67	6.25	1.47	-546.698	1.481	-501.631	10.730
4000	1	2.78	11.00	1.49	-552.828	.504	-481.809	9.645
4000	0.9	3.09	16.61	1.53	-554.358	.888	-457.941	8.920
4000	0.8	3.48	28.97	1.52	-547.650	.958	-398.168	7.925
4000	0.7	3.98	48.94	1.63	-548.879	.749	-327.888	7.380
4000	0.6	4.64	92.48	1.45	-513.510	.814	-155.583	5.685
4000	0.5	5.57	191.05	1.49	-439.858	2.210	176.347	5.289
6000	1.12	2.67	10.62	1.44	-478.353	1.915	-401.799	10.581
6000	1	2.78	16.13	1.50	-482.306	2.106	-378.235	9.875
6000	0.9	3.09	24.86	1.45	-489.958	2.629	-345.640	8.816
6000	0.8	3.48	38.79	1.50	-483.993	2.584	-283.799	8.150
6000	0.7	3.98	62.61	1.93	-483.318	7.981	-200.621	11.814
6000	0.6	4.64	110.16	1.58	-452.169	3.583	-25.812	7.077
6000	0.5	5.57	205.67	1.56	-391.728	1.085	271.648	5.140

FIGURE 4.1 $CaSiO_3$ liquid structure at 3000 K and (a) $V=V_x$ (b) $V=V_x/2$. In blue are the Si-O polyhedra and in light blue are the Ca ions. The black dashed line indicates the primary simulation cell.

(a)

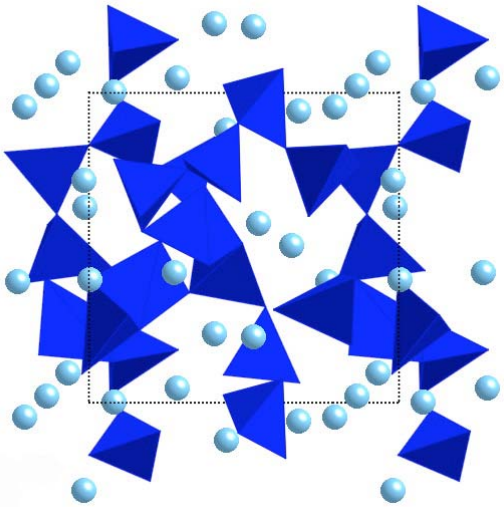

(b)

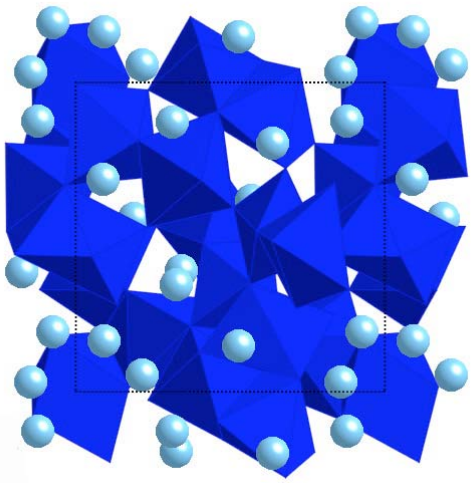

FIGURE 4.2 Si-O coordination number of $CaSiO_3$ liquid at 3000 K (blue symbols), 4000 K (green symbols), and 6000 K (red symbols). The dashed lines are the temperature-averaged Si-O coordination number in $CaSiO_3$ liquid (red), $MgSiO_3$ liquid (blue), and $CaMgSi_2O_6$ liquid (green).

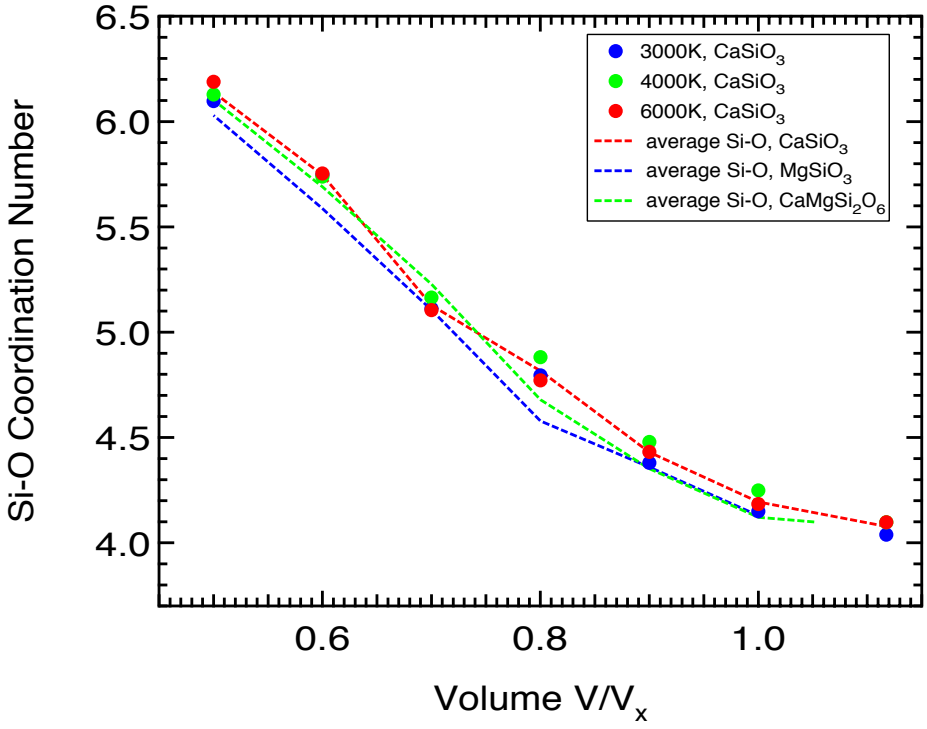

FIGURE 4.3 Ca-O coordination number of $CaSiO_3$ at 3000 K (blue symbols), 4000 K (green symbols), and 6000 K (red symbols). The dashed lines are the temperature-averaged Ca-O coordination number of $CaSiO_3$ liquid (red), and $CaMgSi_2O_6$ liquid (blue).

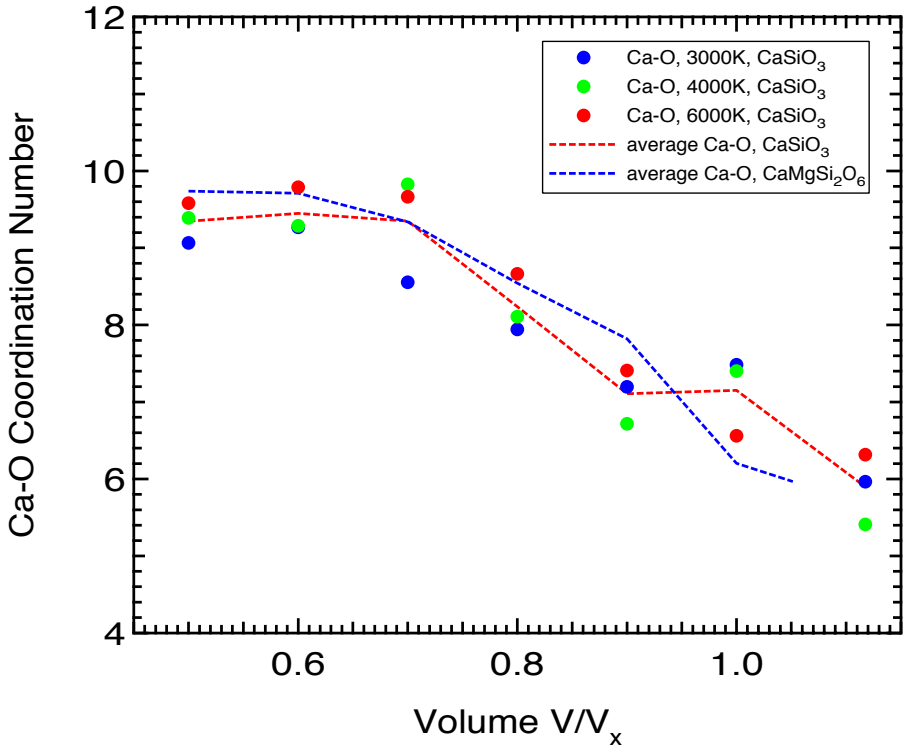

FIGURE 4.4 Si-O coordination distribution in $CaSiO_3$ liquid at (a) 3000K, (b) 4000 K, and (c) 6000 K. The labels indicate the Si-O coordination number.

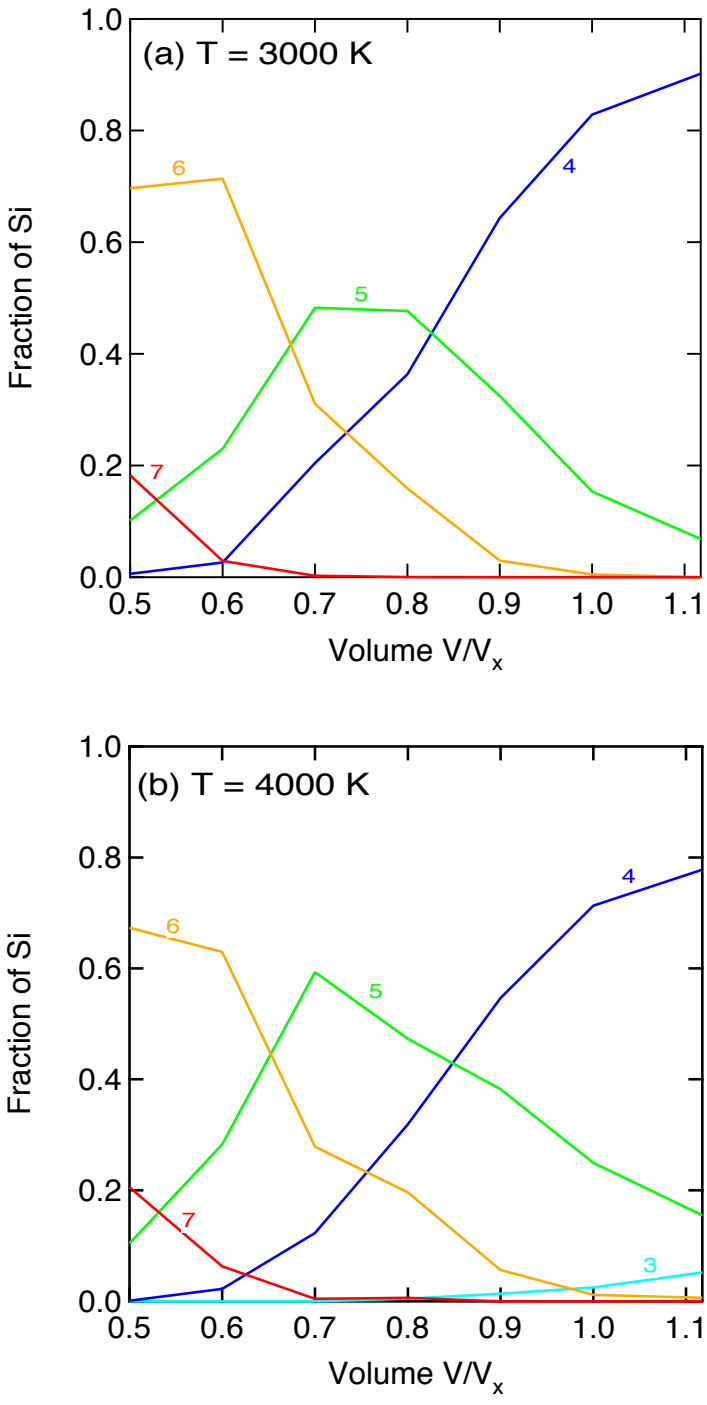

FIGURE 4.4 (continued)

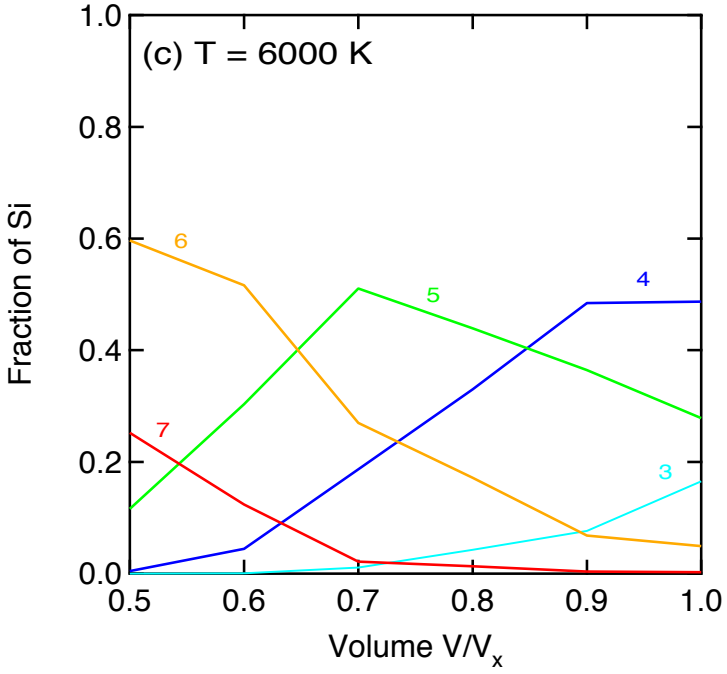

FIGURE 4.5 Equation of state of $CaSiO_3$ liquid. FPMD results (solid symbols) and the Mie-Grüneisen equation of state (curves) fit to the FPMD results at 3000K (blue), 4000 K (green), and 6000 K (red). The uncertainties are within the size of the symbols. The inset is the comparison between simulation results and experimental results at V = 86.9 cm^3/mol, the experimental volume of wollastonite liquid at the ambient-pressure melting point, 1817K (Lange and Carmichael, 1987). The shading represents uncertainty in the extrapolation of the experimental measurements. The open circles are simulation results.

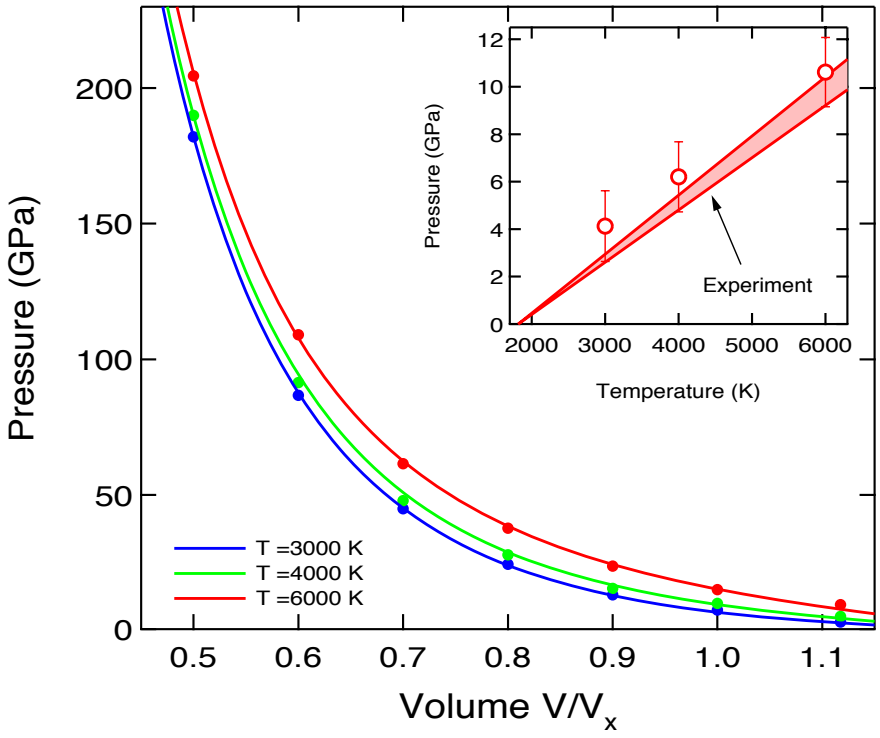

FIGURE 4.6 Grüneisen parameter, γ, as a function of volume. The open circles are the FPMD results and the square is experimental result (Ai and Lange, 2007; Lange, 1997; Lange and Navrotsky, 1992).

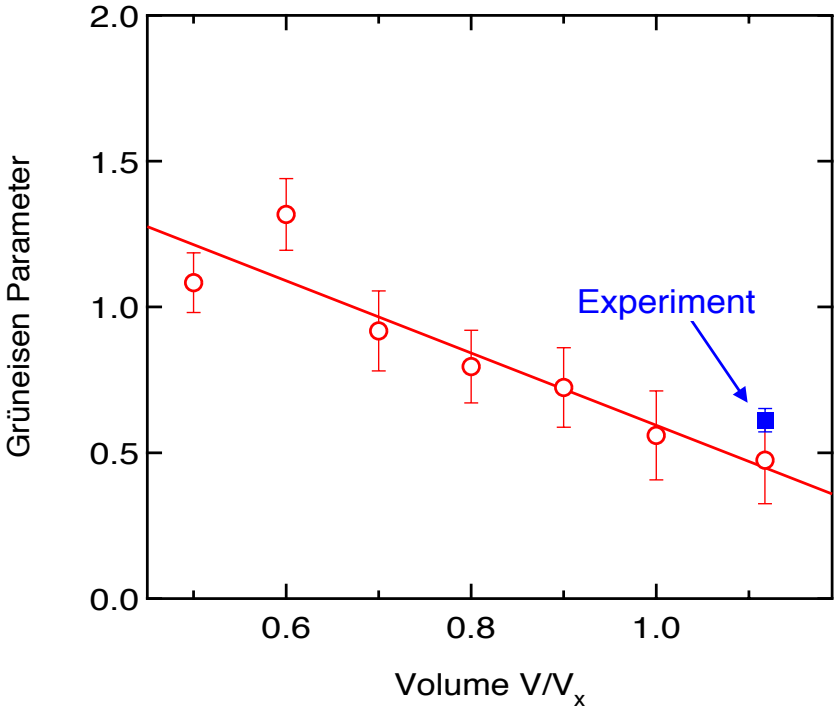

FIGURE 4.7 Heat capacity, C_V, as a function of volume. The open circles are the FPMD results, the square is from (Stebbins et al., 1984), and the solid circle is from (Lange and Navrotsky, 1992).

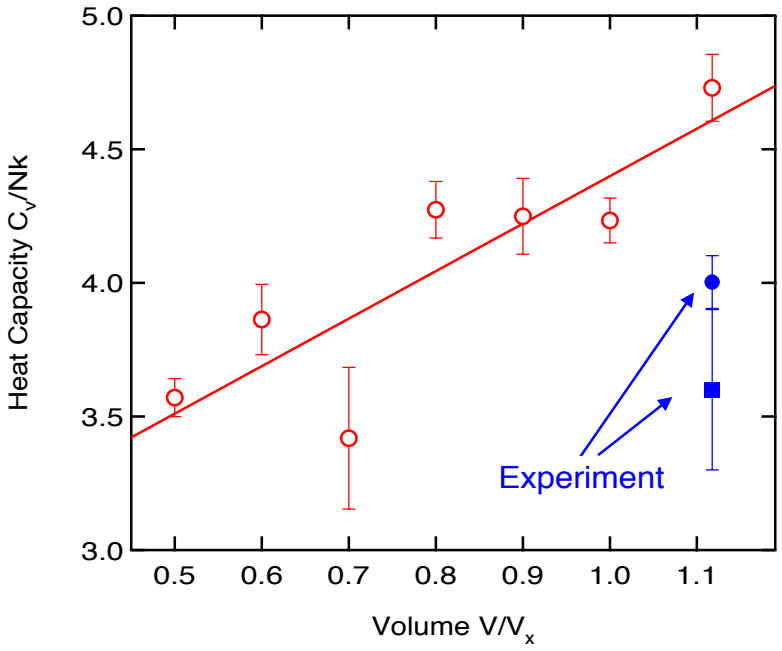

FIGURE 4.8 Equation of state of enstatite (blue), diopside (red), and wollastonite (green) compositions (open symbols and lines) and (inset) the volume of solution at 3000 K (solid line) and its uncertainty (shading) from FPMD simulations.

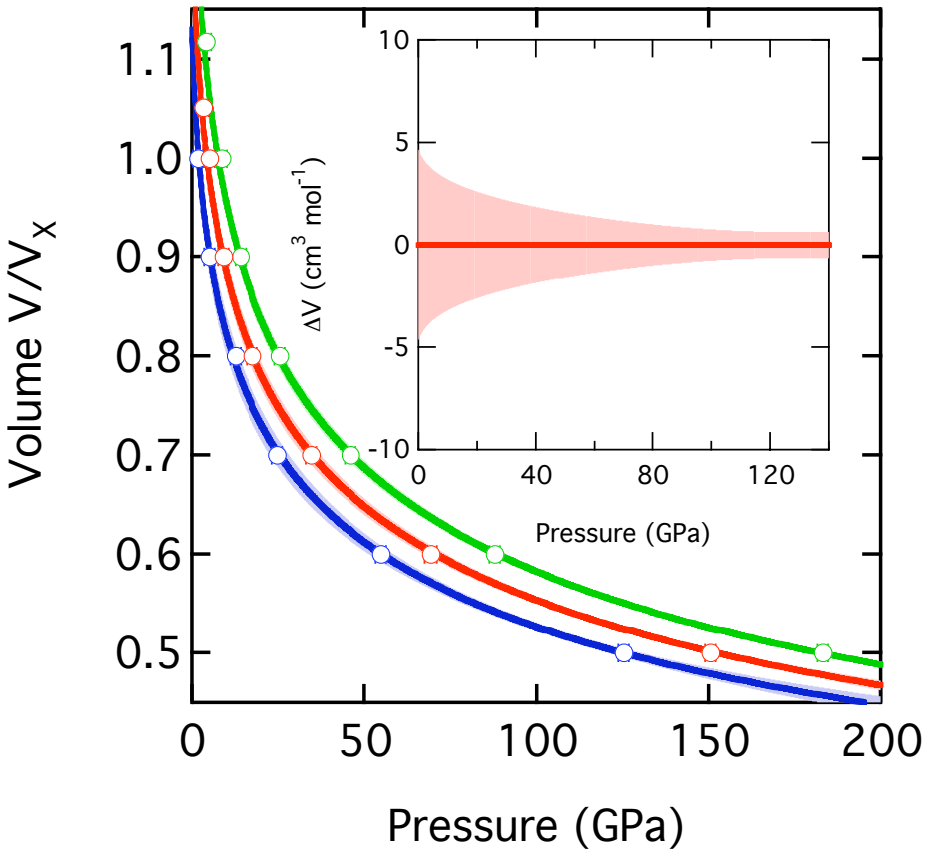

References

Adams, D.J. and Oganov, A.R., 2006. *Ab initio* molecular dynamics study of $CaSiO_3$ perovskite at P-T conditions of Earth's lower mantle. Physical Review B, 73: 1841006.

Ai, Y. and Lange, R.A., 2007. The compressibility of CaO-MgO-Al_2O_3-SiO_2 liquids from new acoustic velocity measurements: reevaluation of the equation of state of $CaMgSi_2O_6$-$CaAl_2Si_2O_8$ liquids to 25 GPa. Journal of Geophysical Research, In Press.

Caracas, R. and Wentzcovitch, R., 2005. $CaSiO_3$ perovskite at lower mantle pressures. Geophysical Research Letters, 32: 1029.

Flyvbjerg, H. and Petersen, H.G., 1989. Error-estimates on averages of correlated data. Journal of Chemical Physics, 91(1): 461-466.

Funamori, N., Yamamoto, S., Yagi, T. and Kikegawa, T., 2004. Exploratory studies of silicate melt structure at high pressures and temperatures by in situ X-ray diffraction. Journal of Geophysical Research, 109: B03203.

Jung, D.Y. and Oganov, A.R., 2005. *Ab initio* study of the high-pressure behavior of $CaSiO_3$ perovskite. Physics and Chemistry of Minerals, 32: 146-153.

Kohn, W. and Sham, L.J., 1965. Self-consistent equations including exchange and correlation effects. Physical Review, 140: A1133–A1138.

Kresse, G. and Furthmüller, J., 1996a. Efficiency of ab-initio total energy calculations for metals and semiconductors. Computational Material Science, 6: 15-50.

Kresse, G. and Furthmüller, J., 1996b. Efficient iterative schemes for ab-initio total energy calculations using a plane-wave basis set. Physical Review B, 54: 11,169–11,186.

Kresse, G. and Hafner, J., 1993. Ab initio molecular-dynamics for liquid metals. Physical Review B, 47: 558–561.

Lange, R.A., 1997. A revised model for the density and thermal expansivity of K_2O-Na_2O-CaO-MgO-Al_2O_3-SiO_2 liquids from 700 to 1900 K: extension to crustal magmatic temperatures. Contributions to Mineralogy and Petrology, 130: 1-11.

Lange, R.A. and Carmichael, I.S.E., 1987. Densities of Na_2O-K_2O-MgO-FeO-Fe_2O_3-Al_2O_3-TiO_2-SiO_2 liquids – new measurements and derived partial molar properties. Geochimica et Cosmochimica Acta, 51: 2931-2946.

Lange, R.A. and Navrotsky, A., 1992. Heat capacities of Fe_2O_3-bearing silicate liquids. Contributions to Mineralogy and Petrology, 110: 311-320.

Li, L. et al., 2006a. Elasticity of $CaSiO_3$ perovskite at high pressure and high temperature. 155: 249-259.

Li, L. et al., 2006b. Phase stability of $CaSiO_3$ perovskite at high pressure and temperature: Insights from as initio molecular dynamics. Physics of the Earth and Planetary Interiors, 155: 260-268.

Nose, S., 1984. A molecular-dynamics method for simulations in the canonical ensemble. Molecular Physics, 52(2): 255-268.

Rigden, S.M., Ahrens, T.J. and Stolper, E.M., 1989. High pressure equation of state of molten anorthite and diopside. Journal of Geophysical Research, 94: 9508-9522.

Shim, S.-H., Duffy, T.S. and Shen, G., 2000. The equation of state of $CaSiO_3$ perovskite to 108 GPa at 300 K. Physics of the Earth and Planetary Interiors, 120: 327-338.

Shim, S.-H., Jeanloz, R. and Duffy, T.S., 2002. Tetragonal Structure of $CaSiO_3$ perovskite above 20 GPa. Geophysical Research Letters, 29(24): 2166.

Smyth, J.R. and McCormick, T.C., 1995. in Mineral Physics and Crystallography: A Handbook of Physical Constants. In: T.J. Ahrens (Editor), AGU Reference Shelf 2. American Geophysical Union, Washington, DC.

Stebbins, J.F., Carmichael, I.S.E. and Moret, L.K., 1984. Heat Capacities and entropies of silicate liquids and glasses. Contribution to Mineralogy and Petrology, 86: 131-148.

Stebbins, J.F. and McMillan, P., 1989. Five- and six-coordinated Si in $K_2Si_4O_9$ glass quenched from 1.9 GPa and 1200 ^oC. American Mineralogist, 74: 965-968.

Stixrude, L., Cohen, R.E., Yu, R. and Karkauer, H., 1996. Prediction of phase transition in $CaSiO_3$ perovskite and implications for lower mantle structure. American Mineralogist, 81: 1293-1296.

Stixrude, L. and Karki, B., 2005. Structure and freezing of $MgSiO_3$ liquid in Earth's lower mantle. Science 310: 297-299.

Stixrude, L., Lithgow-Bertelloni, C., Kiefer, B. and Fumagalli, P., 2007. Phase stability and shear softening in $CaSiO_3$ perovskite at high pressure. Physical Review B, 75: 024108.

Sun, N., Stixrude, L. and Karki, B.B., 2008a. High pressure structure and equation of state of diopside liquid. Earth and Planetary Science Letters, to be submitted.

Sun, N., Stixrude, L.P. and Karki, B.B., 2008b. Dynamics of diopside liquid at high pressures. to be submitted.

Williams, Q. and Garnero, E.J., 1996. Seismic evidence for partial melt at the base of Earth's mantle. Science, 273(5281): 1528-1530.

Xue, X., Stebbins, J.F., Kanzaki, M. and Tronnes, R.G., 1989. Silicon coordination and speciation changes in a silicate liquid at high pressures. Science, 245: 962-964.

Zhang, Y., Zhao, D., Matsui, M. and Guo, G., 2006. Equation of state of $CaSiO_3$ perovskite: a molecular dynamics study. Physics and Chemistry of Minerals, 33: 126-137.